Geophys. J. Int. (1990) **101**, 89–110

Crust and upper mantle structure along the DSS Baltic profile in SE Finland

U. Luosto,[1] T. Tiira,[1] H. Korhonen,[1] I. Azbel,[2] V. Burmin,[3] A. Buyanov,[2] I. Kosminskaya,[3] V. Ionkis[2] and N. Sharov[2]

[1] *Institute of Seismology, University of Helsinki, Et. Hesperiankatu 4, SF-00100 Helsinki, Finland*
[2] *Institute of Geology, USSR Acad. Sci. Kola Branch, 184200 Apatity, USSR*
[3] *Institute of Physics of the Earth, USSR Acad. Sci., B. Gruzinskaya 10, 123810 Moscow, USSR*

Accepted 1989 September 29. Reveived 1989 September 18; in original form 1989 April 4

SUMMARY

The 430 km long DSS Baltic profile in SE Finland runs through the Rapakivi intrusion, the Svecokarelian geosynclinal complex, including the Ladoga–Bothnian Bay zone, and the Archean basement complex. A brief description of field operations in 1982 is presented. Record sections of *P*- and *S*-waves were used for the interpretations. A starting model was constructed by inverse methods and improved by dynamic ray tracing modelling. Three blocks are indentified on the cross-section from SW to NE. These are the southern, associated with the Rapakivi Massif, depth to Moho (*M*) about 40 km; the central, Ladoga–Bothnian Bay zone, with *M* of approximately 55–60 km, and the northern, Archean crystalline basement, with *M* about 40–45 km. The average crustal velocity is 6.6–6.7 km s^{-1}. The crustal structure along the Baltic profile is compared with the surrounding DSS profiles, Finnish Sveka and Soviet Kem–Tulos and Ladoga profiles. The eastern border of the Ladoga–Bothnian Bay zone was located and specific features of the crust and uppermost mantle along the profile area are discussed.

Key words: deep seismic sounding, Fennoscandian Shield, Ladoga–Bothnian Bay zone, lithospheric structure, Rapakivi intrusion.

INTRODUCTION

Investigations of the crustal structure of Finland are contributing to a more exact understanding of the evolution and tectonics of Fennoscandia. The Baltic profile is located in SE Finland. It completes the substantial Finnish and Soviet network in the SE Fennoscandian Shield (Litvinenko *et al.* 1981, 1987; Litvinenko 1984; Luosto *et al.* 1984; Luosto 1986; Luosto & Korhonen 1986; Grad & Luosto 1987).

The participants in the 1982 field work were from Finland, USSR, Sweden and FRG. The tectonic sketch map (Fig. 1) shows a 430 km long profile (No. 1 in Fig. 1) crossing three geological provinces from north to south, namely, the Karelian province in the Archean Domain (2.5–2.8 Ga) the Svencofennian or Svecokarelian geosynclinal complex (1.8–1.9 Ga), and the Rapakivi intrusion in the south (1.5–1.7 Ga). Seven shotpoints A, B, . . . , G were set up at 30–100 km spacing along the profile line with a distance between receivers of 2 km on average. The shots were fired at sea (A, B), in small lakes (C, . . . , G) or in a quarry, i.e. blasts in the Kostamuksha quarry (H) were used. For other details see Table 1.

The shots were recorded by a total of 48 stations, 36 three-component stations, 16 'MARS 66' stations (Berckhemer 1970), 10 'ASS' (Zverev *et al.* 1978) and 10 'SN-PCM80' (Nurminen & Hannula 1981), and 12 six-channel stations, 10 'Taiga-2' and two 'SN-PCM-80'. The analogue records were digitized, and record sections for *P*- and *S*-waves were compiled. A more detailed description of the field work as well as the first results for the interpretation by conventional DSS methods were published earlier by Luosto *et al.* (1985) and by Korhonen *et al.* (1986).

This paper gives a more detailed account of the interpretation and also the results obtained by dynamic ray tracing and generalized inversion.

P-WAVE FIELD

The signal-to-noise ratios in the records of the main profile from all the shotpoints were high, making possible phase

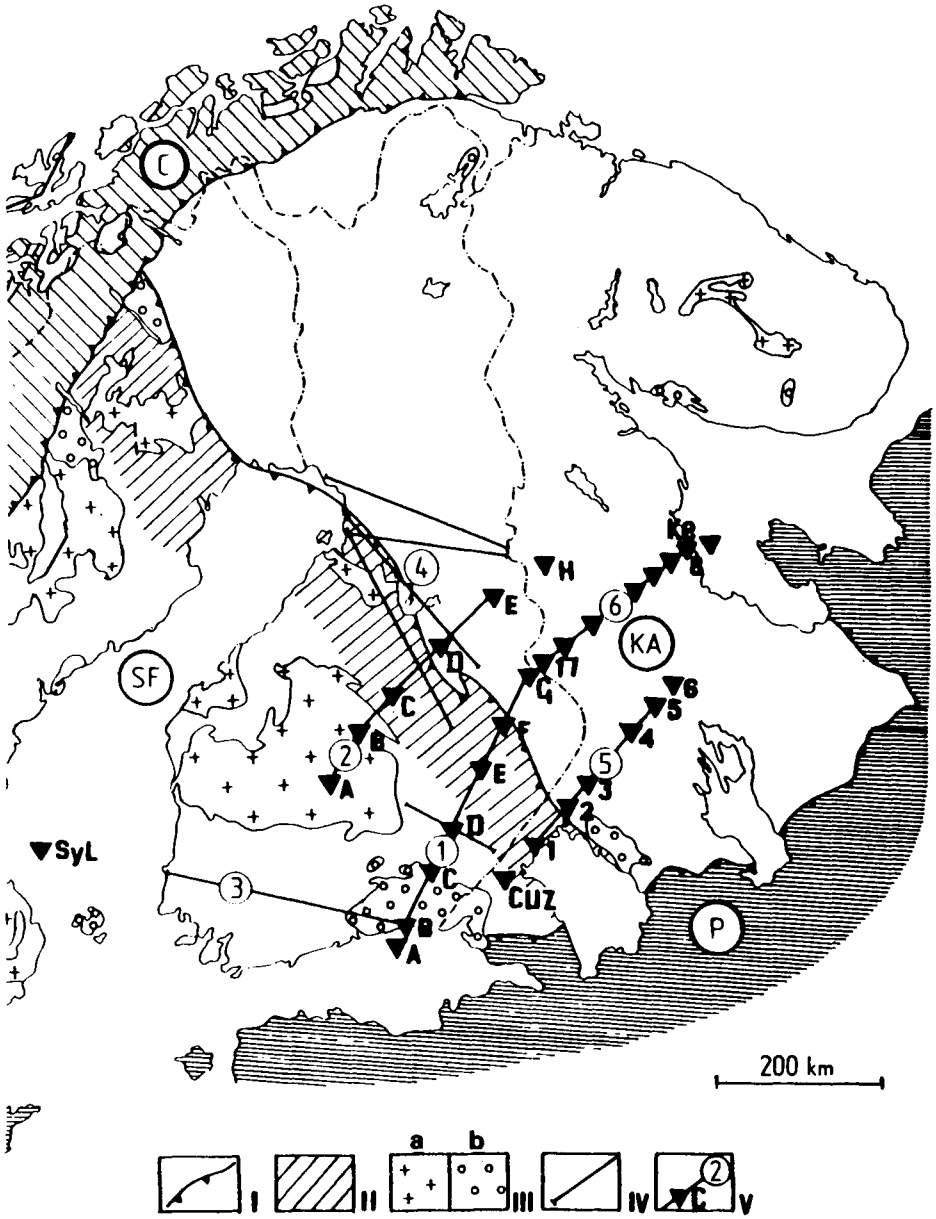

Figure 1. Location of DSS profiles in SE part of the Fennoscandian Shield: 1—Baltic, 2—Sveka, 3—Sylen–Porvoo, 4—Bothnian quarry blast profiles, 5—Ladoga, 6—Kem–Tulos. Tectonic provinces: C—Calendonides, KA—Karelian, SF—Svecofennian, P—Palaeozoic platform cover. I—Borders of main tectonic provinces; II—Ladoga–Bothnian bay zone; III—Proterozoic granites 1900–1800 Ma (a), 1700–1500 Ma (b), IV—DSS profile; V—shotpoint on the profile.

correlations of the first arrivals on sufficiently long (several tens of kilometres) intervals of the profile. At the same time, the record sections show considerable variations in the later arrivals, which are probably connected with reflected waves. In the observed wavefield (see Figs 2–8) with a reduction velocity of $v_R = 8.0\ km\ s^{-1}$ two groups are clearly seen as first arrivals: crustal waves with velocities of $6.0–7.0\ km\ s^{-1}$ and mantle waves with velocities of more than $8.0\ km\ s^{-1}$. Two systems of traveltime curves of refracted and reflected *P*-waves were constructed (Figs 9 and 10). On the basis of phase correlation, several main groups of waves having common points could be identified between the shotpoints. The correlated crustal waves can roughly be divided into four groups with the following velocities: P_0—5.8–6.1; P_1—6.2–6.3; P_2—6.4–6.6; P_3—6.9–$7.3\ km\ s^{-1}$.

Refracted mantle waves P_M with velocities of more than $8\ km\ s^{-1}$ can clearly be traced for points A, B, and C. Their distinguishing characteristic is a long cross-over distance of 210–280 km. The recording range of mantle waves is about 200 km for points A and B. At distances over 300 km (shotpoint A), the velocities of the mantle waves are somewhat higher than $8.0\ km\ s^{-1}$.

The appearance of the first mantle waves in the south and the corresponding branches of traveltime curves from shotpoints E, F, and G have a completely different character from those in the north. The traveltimes of crustal waves (Fig. 10) of distances over 100 km are about 1 s greater than

Table 1. Shot sizes (ton) on the Baltic profile and timetable of shots.

No.	Shot point	A	B	C	D	E	F	G	H (Kostamuksha)		
	Coordi- φ	60°9'	60°21'	61°10'	61°35'	62°20'	62°57'	63°35'	64°41'		
	nates λ	26°17'	26°35'	26°59'	27°55'	28°51'	29°26'	30°3'	30°38'		
	Water depth (m)	50	20	8	10	6	5	8	Hole depth (m) 15		
	Time (local)	00.30	00.50	01.10	01.30	01.50	02.10	02.30	14.00		
	Date 1982	Size	Size	Size	Size	Size	Size	Size	Date	Size	Retardation (s)
0	3.8					0.7			30.7	216	0.84
1	5.8	1.0	1.0	1.36	1.36	0.7	0.4	0.3	-	-	-
2	7.8	1.0	1.0	1.36	0.72	0.3	0.4	0.9	6.8	270	1.50
3	9.8	0.75	1.0	0.72	0.3	0.5	0.9	1.36	-	-	-
4	11.8	0.5	0.8	0.4	0.3	0.72	1.36	1.36	-	-	-
5	13.8	0.25	0.5	0.4	0.72	1.36	1.36	1.7	13.8	265	1.26
6	-	-	-	-	-	-	-	-	20.8	181	1.40

those from shotpoints A and B. Sharp changes in the slope of traveltime curves of the first arrivals occur, with apparent velocities changing from 6.7–7.1 to about 9.0 km s^{-1}. The times of the parallel traveltime curves of E, F, and G coincide at reciprocal points with the times for branches A and B in the northern part of the profile (Fig. 9). For shotpoint E to the south, which was closer to shotpoints A and B, we can still trace mantle waves with a lower apparent velocity of about 8.4 km s^{-1}. In the case of shotpoint H (see Fig. 11a), the observations started at a distance of 120 km. Up to 180 km the velocity of first arrivals is about 6.4 km s^{-1} and between 180 and 220 km it is 6.7 km s^{-1}. In the distance range of 220–260 km, mantle waves have a velocity of about 8 km s^{-1}, increasing to 8.5 km s^{-1} at 260–320 km. Complicated mantle waves with increased velocities at distances greater than 300 km could only be explained after ray tracing modelling as the refracted waves are associated with a boundary deeper than the Moho (M) discontinuity.

It must be noted that there is an instability associated with the tracing of reflected waves along the different parts of the profile for boundaries within the crust. Although in some cases the fragments of their traveltime branches were sufficiently well correlated for both crustal and mantle waves in the record sections e.g. for points A, B, C, D (Fig. 10, Figs 2–5), all these reflected waves are not related to refracted waves which were clearly discernible in the field of crustal waves. On the other hand there are record sections, for instance, the southern branch from shotpoints E and F, and the northern branch from shotpoint C at distances of 160–180 km from the shotpoints, where it is difficult to observe any stable coherent reflections, whereas at distances between 200 and 300 km for shotpoints F and G we can observe as later arrival well-defined intense reflections with reduced times of 9–10 s. In spite of clear reflections on record sections for shotpoints A and B, C_N (from C to north) and D_N, it was not easy to connect them with refracted waves recorded from shotpoints F, G and H.

The main parameters of observed refracted *P*- and *S*-waves for all the shotpoints are given in Table 2 and those of the reflected waves in Table 3.

AMPLITUDE CURVES OF *P*-WAVES

To characterize the signal levels recorded from different shotpoints and the dynamic features of the first arrivals, the amplitude curves for the first maxima of *P*-waves in the vertical component have been plotted using the records obtained from 50 Soviet stations. Fig. 12 shows the averaged and smoothed amplitude curves for all the shotpoints as a function of distance from the source.

The charges of shotpoints A and B fired in the sea produced much higher signal levels than the lake shots E, F and G of an approximately similar size (see Fig. 12 and Table 1). This is probably due to the fact that the depths in the sea were greater even though a technique of distributed charges for explosions in shallow waters was applied in the lakes (see Burkhardt & Vees 1975). Optimal depths for the sea shots were not achieved in the sea, either. The higher amplitudes of records from shotpoint B compared with those from A in deeper water can be explained to be only due to a source effect. The frequency contents of records from shotpoints A and B are clearly different. The predominant frequencies on the records for shotpoints A and B independent of shot size are about 6 and 9 Hz, respectively. Probably water depth together with the thickness of sedimentary layers and other geological conditions in the source area essentially affect the frequency content and amplitudes of the source signals.

Despite the above differences in amplitude curves, branches P_1, P_2 and P_3 for crustal waves and P_{M1} and P_{M2} for mantle waves can easily be distinguished. The differences in amplitude levels and slopes are large. Thus in the cases of shotpoints C, E, F and G the amplitudes of the P_1-waves decrease by a factor of 10 over the first 50 km. The amplitudes of P_2-waves become 5–7 times smaller in a 100 km interval while on the contrary P_3-waves, have a higher intensity than P_2-waves. This distance range is characterized by oscillating curves where the local maxima most probably belong to the critically reflected rather than the refracted waves. All the curves illustrate a decrease in amplitudes at the cross-over distance from the crustal to the

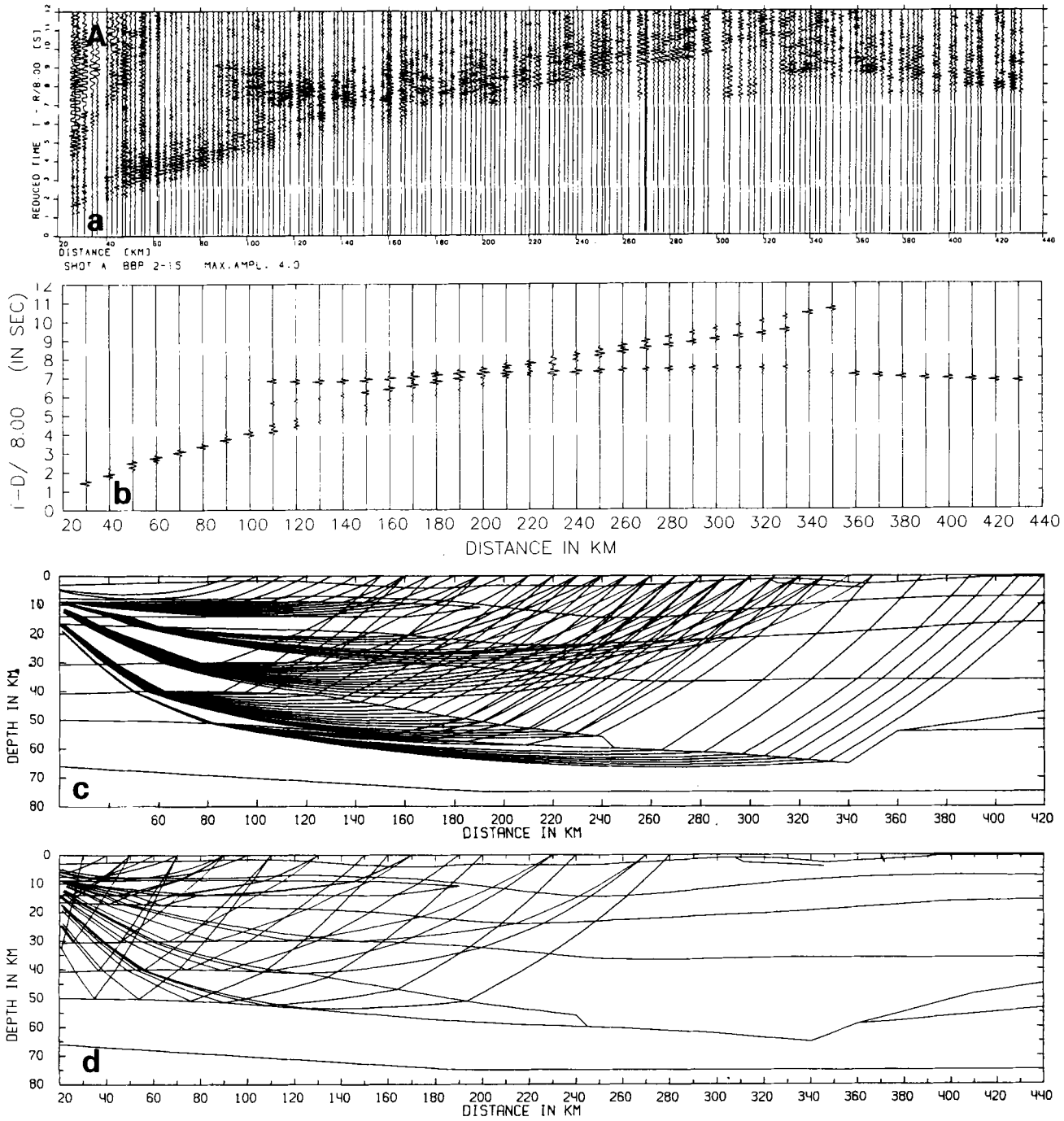

Figure 2. The 2-D modelling for shotpoints A–G along the Baltic profile, (a) amplitude normalized observed *P*-wave record section, bandwidth of digital filter 2–15 Hz; (b) amplitude normalized synthetic record section; (c) ray paths of the refracted waves; (d) ray paths of reflected waves in the model. Only the velocity discontinuities are shown; the actual velocities can be taken from Fig. 16(a). Distances are measured from shotpoint A.

mantle waves for these shotpoints. The behaviour of the amplitude curves for shotpoints A and B is quite different. Now the amplitudes of P_1- and P_2-waves decrease by a factor of 10 in a distance of about 100 km, local maxima do not exist and a decrease in amplitude at the cross-over distance of the mantle waves is less distinct. However, a distinct decrease is observed at a greater distance, where the transition from the mantle wave P_{M1} as first arrival to P_{M2} is established in high amplification records.

The amplitude curves also enable us to compare the characteristics of the data in various parts of a profile. Thus a complex character of the P_2 amplitude variation for shotpoint C (curve C_N) is obvious in the zone between points E and F. On curve E_S the pronounced amplitude

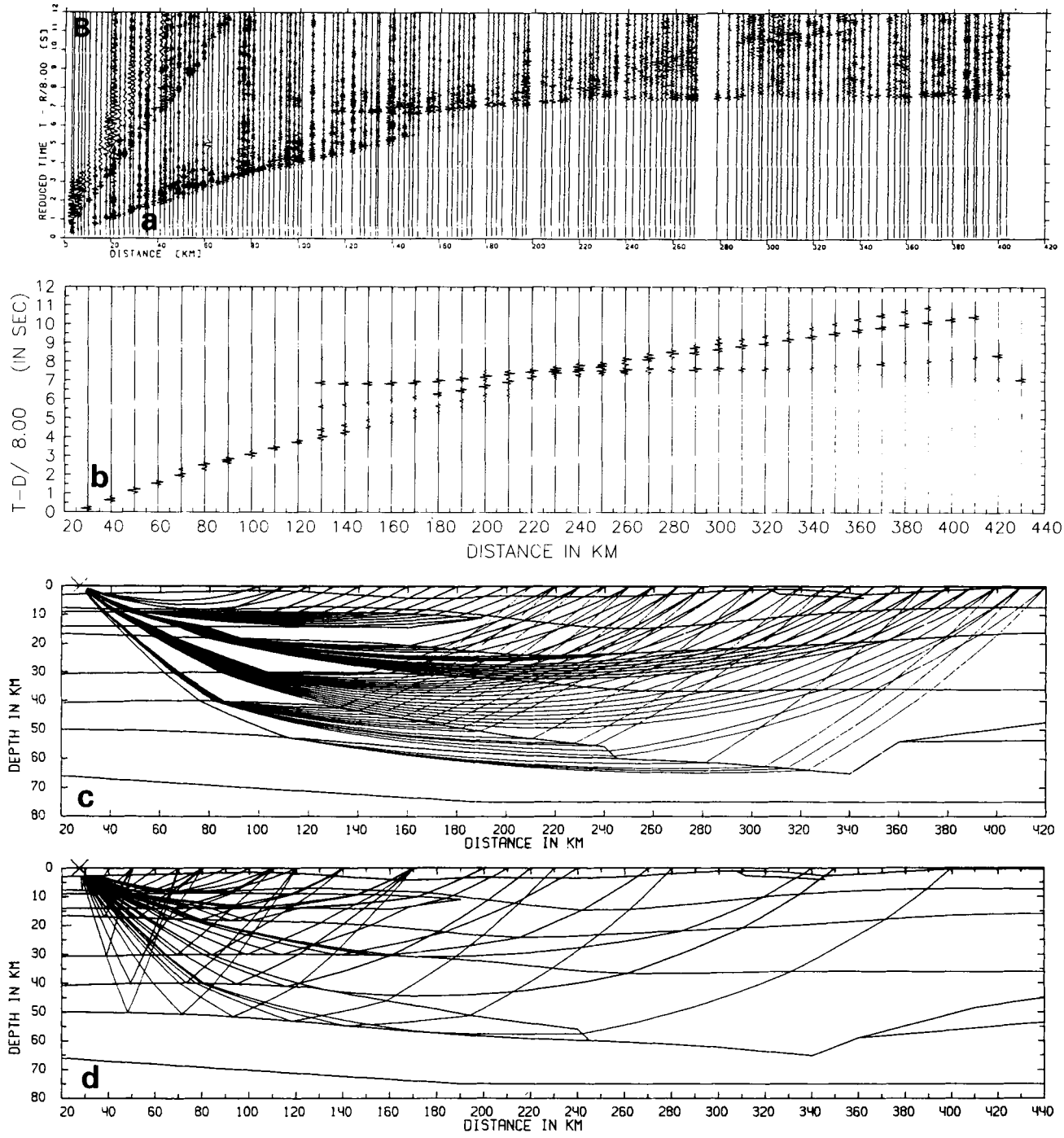

Figure 3. See caption to Fig. 2.

maximum up to a distance of 220 km is evidently due to a strong overcritical reflected P_2-wave very closely approaching the first P_3-waves and thus might not characterize the refracted P_3-wave at all. On the whole, amplitude levels in the 200 km range from the first records decrease by about a factor of 10 for the crustal waves and by a factor of 30–50 for the mantle waves recorded in the 200–400 km range.

The amplitude curves (Fig. 12) provide information about lateral variation of the intensity of crustal and mantle waves in addition to data on relative intensity variations obtained from the trace normalized record sections. The crustal waves dominate in record sections up to the cross-over distance of the mantle waves; the reflected waves reach the amplitude maximum only in the vicinity of the critical angles. At distances greater than the cross-over distance of the mantle waves, the normalized record sections are not able to reflect any variations of the waves because they are almost an order of magnitude less than the largest crustal

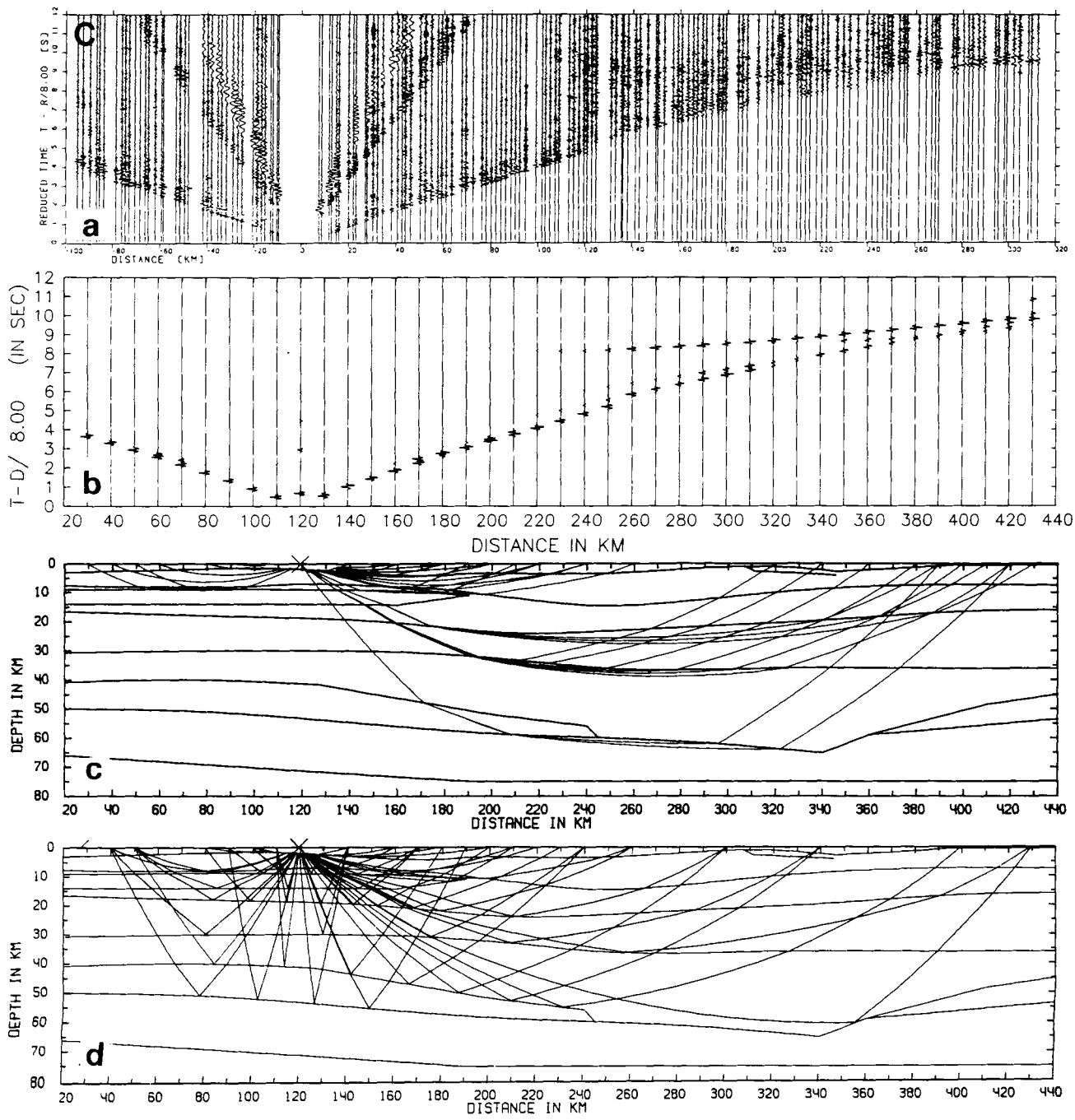

Figure 4. See caption to Fig. 2.

waves used to normalize the seismograms in record sections.

The dynamic behaviour of crustal waves also reveals differences in velocity gradients: in the upper crust there is a considerable attenuation testifying to the high velocity gradients, while in the lower crust the velocity variations are weaker. Some maxima in the amplitude curves are caused by the near-surface geology (e.g. the interval E–F at the profile).

S-WAVE FIELD

The vertical component of the *S*-waves has been analysed in some detail. In general the field of *S*-waves (Fig. 13) is similar to that of the *P*-waves and well correlated reflected *S*-waves have analogies to *P*-waves (Fig. 13). There are, however, some differences between *P*- and *S*-wavefields. The most prominent of these form a more complicated picture of the first *S* arrivals; they show more frequent changes in wave frequency, a sharp decrease in the amplitudes of phases, and a piecewise and echelon character of traveltime curves, which are clearly traceable only up to a distance of about 200 km. The apparent velocity for crustal waves ranges from 3.5 to 3.7 km s^{-1} (see Table 2). The first refracted mantle waves are practically not traceable.

Reflected arrivals are better seen in the *S* field as compared to the *P* field (compare northern branches from

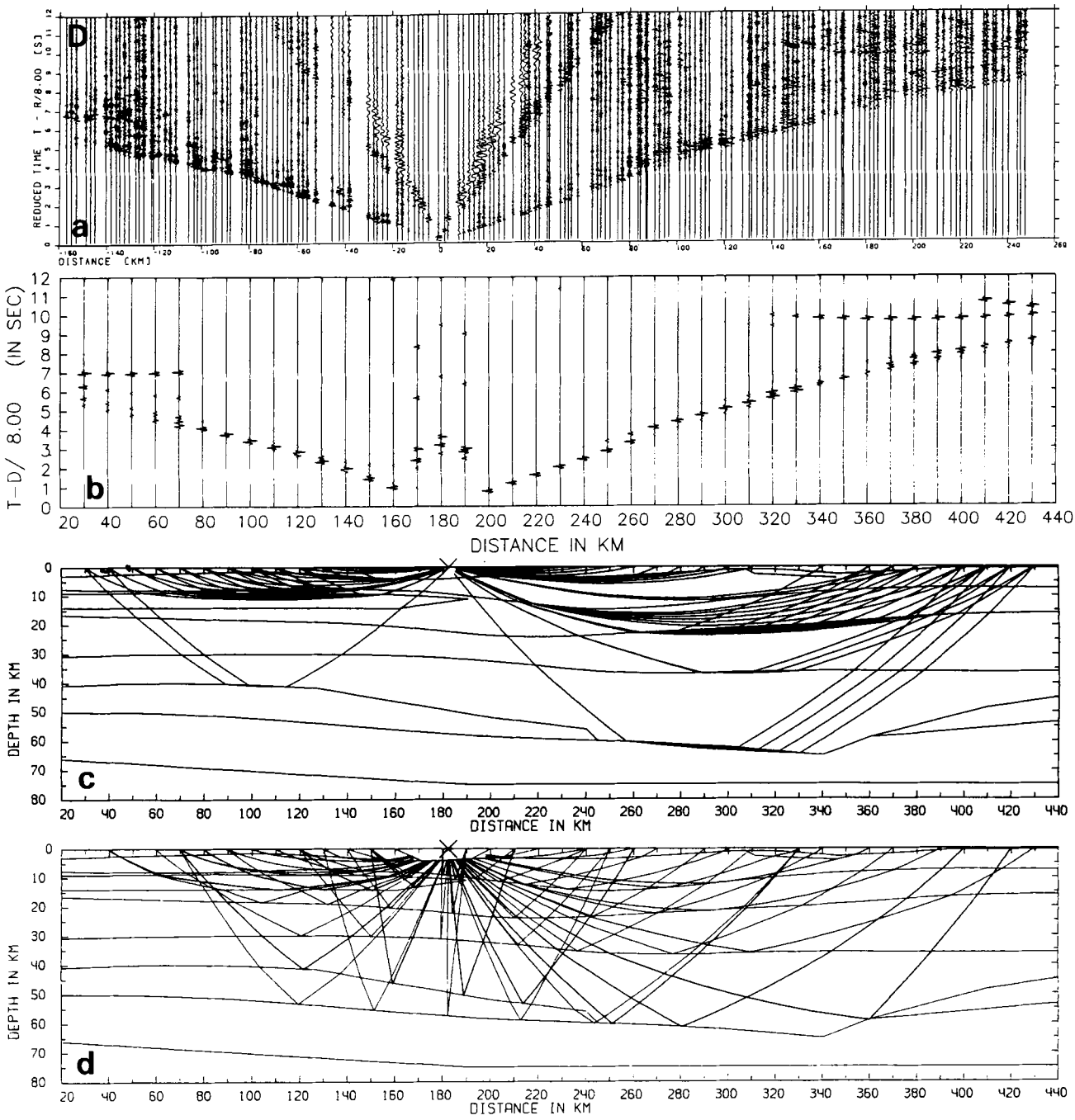

Figure 5. See caption to Fig. 2.

the shotpoint C in *P* and *S* record sections, Figs 4 and 13). The comparison of the records for shotpoints A, B and F, G shows that the northern part of the profile is characterized by more short fragments of intensive reflections in the crustal *S*-wave domain than in the *P*-wave domain.

In the joint analysis of *P*- and *S*-wavefields, the task of determining analogue structural features for crustal and mantle waves is particularly important. For the first arrivals this problem was solved unambiguously since their traveltime branches nearly coincide when the ratio t_S/t_P is taken to be 1.73. Table 2 illustrates a minor but systematic decrease from the standard value of $V_P/V_S = 1.73$ for the first arrivals in the central and northern part at the profile. It also was not difficult to identify the crustal reflections especially for traveltime curves with reciprocal points.

Difficulties arise in identifying the phases of the waves reflected from the mantle. This is especially true for shotpoint B, because the most obvious phases for S^MS-waves arrived more than 1 s late, when a standard value of $V_P/V_S = 1.73$ is assumed. The coincidence of the *P*- and *S*-wave amplitude maxima (see Fig. 12) convinced us that the propagation paths of these waves are the same. In this case we calculated the depths of the boundary independently from the *P* and *S* reflections using the

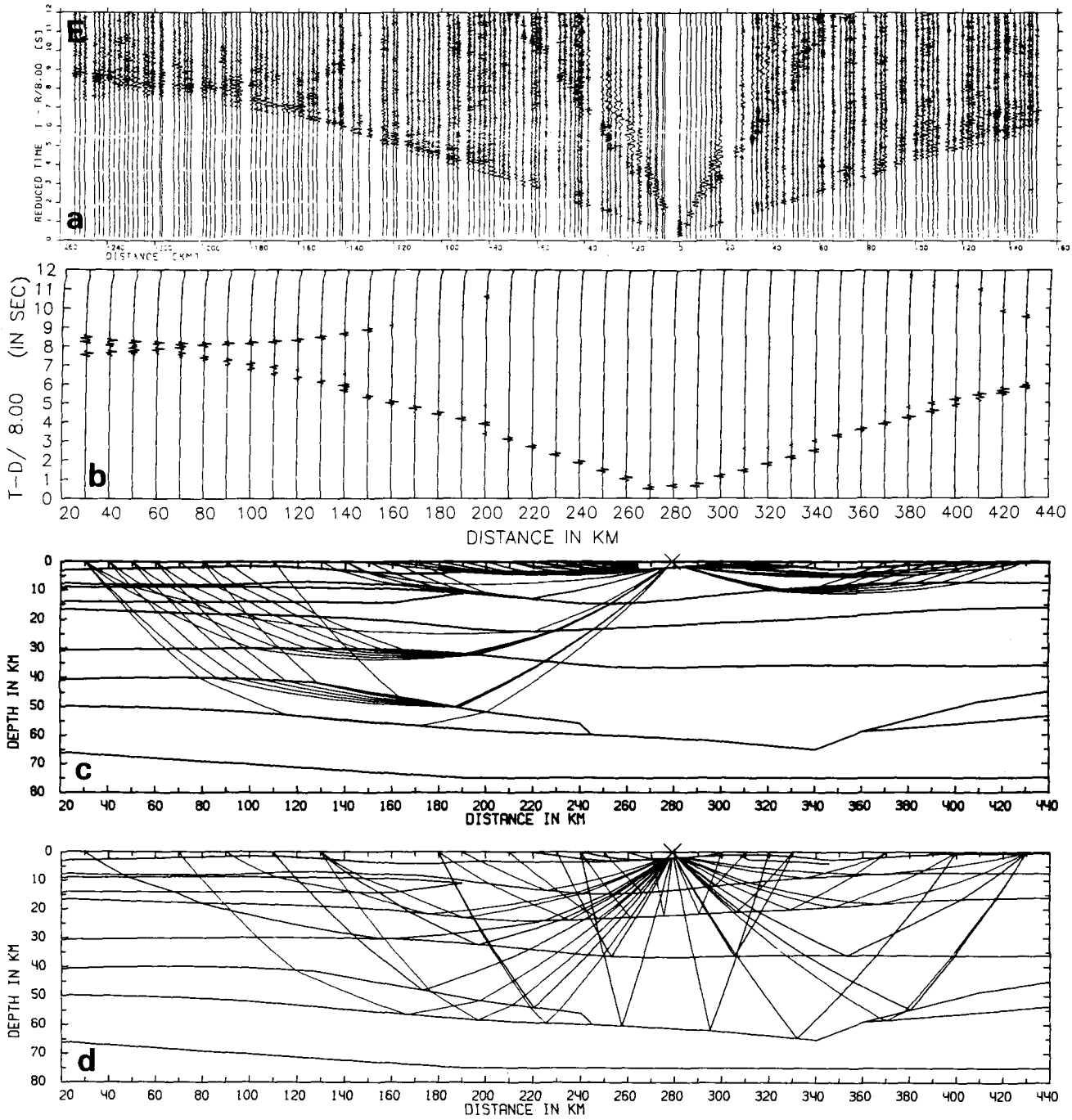

Figure 6. See caption to Fig. 2.

average velocities $\bar{V}_P$ and $\bar{V}_S$. The depth coincidence within the 1–2 km range was considered satisfactory. These estimations enable us to infer that the time discrepancy between the *P*- and *S*-waves along the profile is mainly caused by variations in the parameter V_P/V_s.

Table 3 gives the t_S/t_P values for the major phases of reflected waves which were subsequently used to define the velocity cross-section. The ratio of the times of *S*- and *P*-waves reflected from the M discontinuity varies along the profile. It approaches 1.8, 1.73 and 1.70 for the southern, central and northern parts, respectively. We did not observe residuals between traveltime plots of the refracted or reflected S_x- and S_y-waves versus distance from the source, which would have testified a *S*-wave splitting into S_V and S_H by anisotropy. A complex polarization procedure is obviously necessary to answer this question.

Characteristics of *P*- and *S*-wave arrivals indicate the existence of several crustal layers with the following velocities for the seismic waves: 6.0–6.3 (3.4–3.6), 6.4–6.6 (3.7–3.8) and 6.9–7.3 (3.9–4.0) km s^{-1}. The crust–mantle transition zone has a complex structure and varies along the profile as shown later.

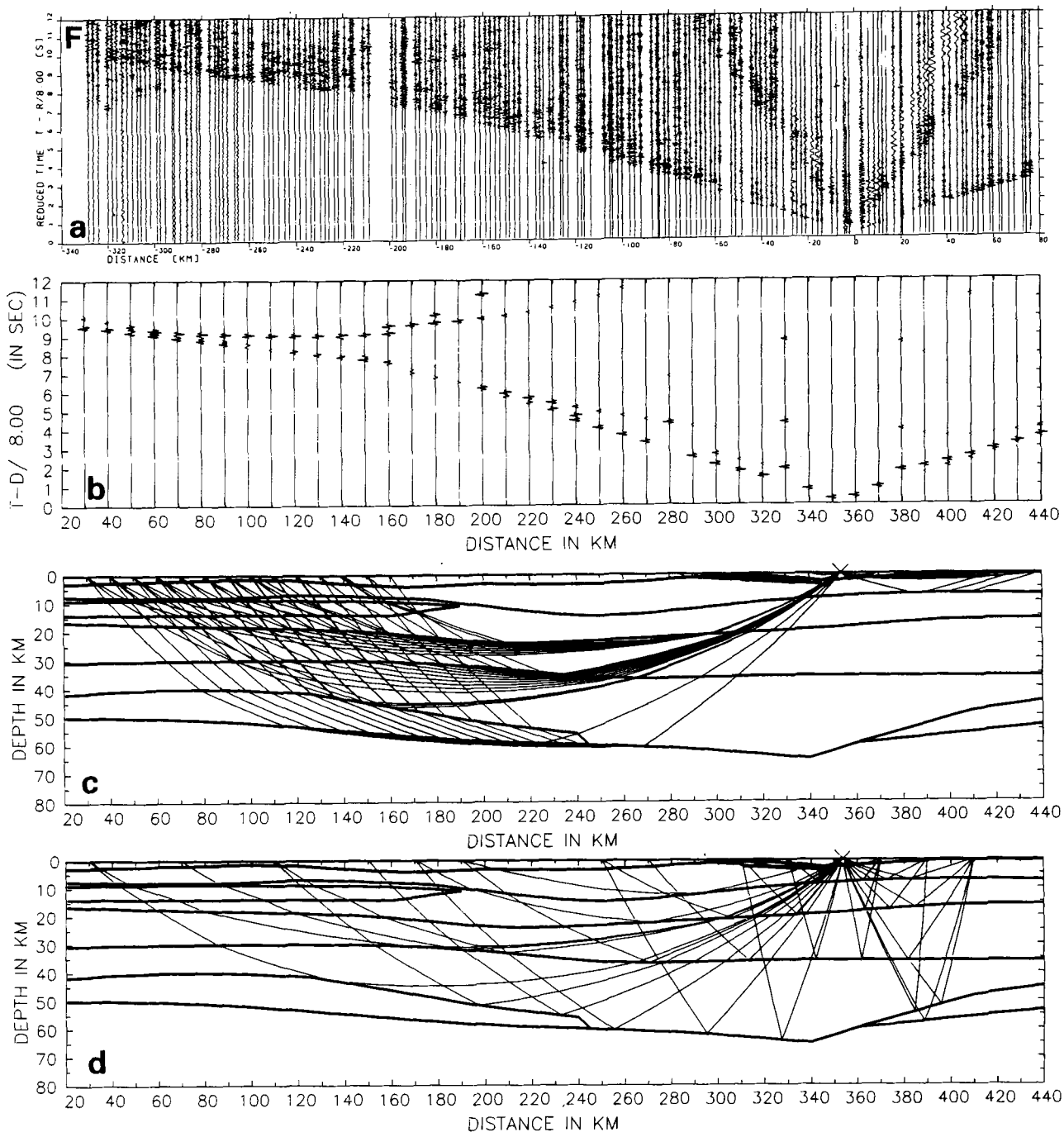

Figure 7. See caption to Fig. 2.

DATA INTERPRETATION

The steps of data processing and interpretation are shown in Fig. 14. The intercept time method (Pavlenkova 1973, 1982) was used to compile the first 2-D model (Fig. 15) by recalculating systems of traveltime curves of refracted waves (see Fig. 9) with different values of reduction velocity V_R for determining the velocity isolines in the plane (X, Z), Fig. 15(a). The depths (Fig. 15c) were computed using average velocity distributions (Fig. 15b), constructed from $V(Z)$ models calculated by Burmin's method (Burmin 1981) for all the shotpoints. These isolines do not correspond to the velocity *in situ* but to the average velocity between the Earth's surface and the isoline. The interfaces included are based on the calculations by the prospecting methods (Puzyrev 1959; Riznichenko 1985). A more complete presentation of these reflectors is shown in Fig. 16(b).

Another model $V(X, Z)$ for the upper crust was derived (Fig. 17) by applying a generalized inversion technique (Buyanov 1986) to the kinematic data of first arrivals of refracted P- and S-waves. The velocity isolines of P- and S-waves (Fig. 17) show the greatest velocity gradients in the

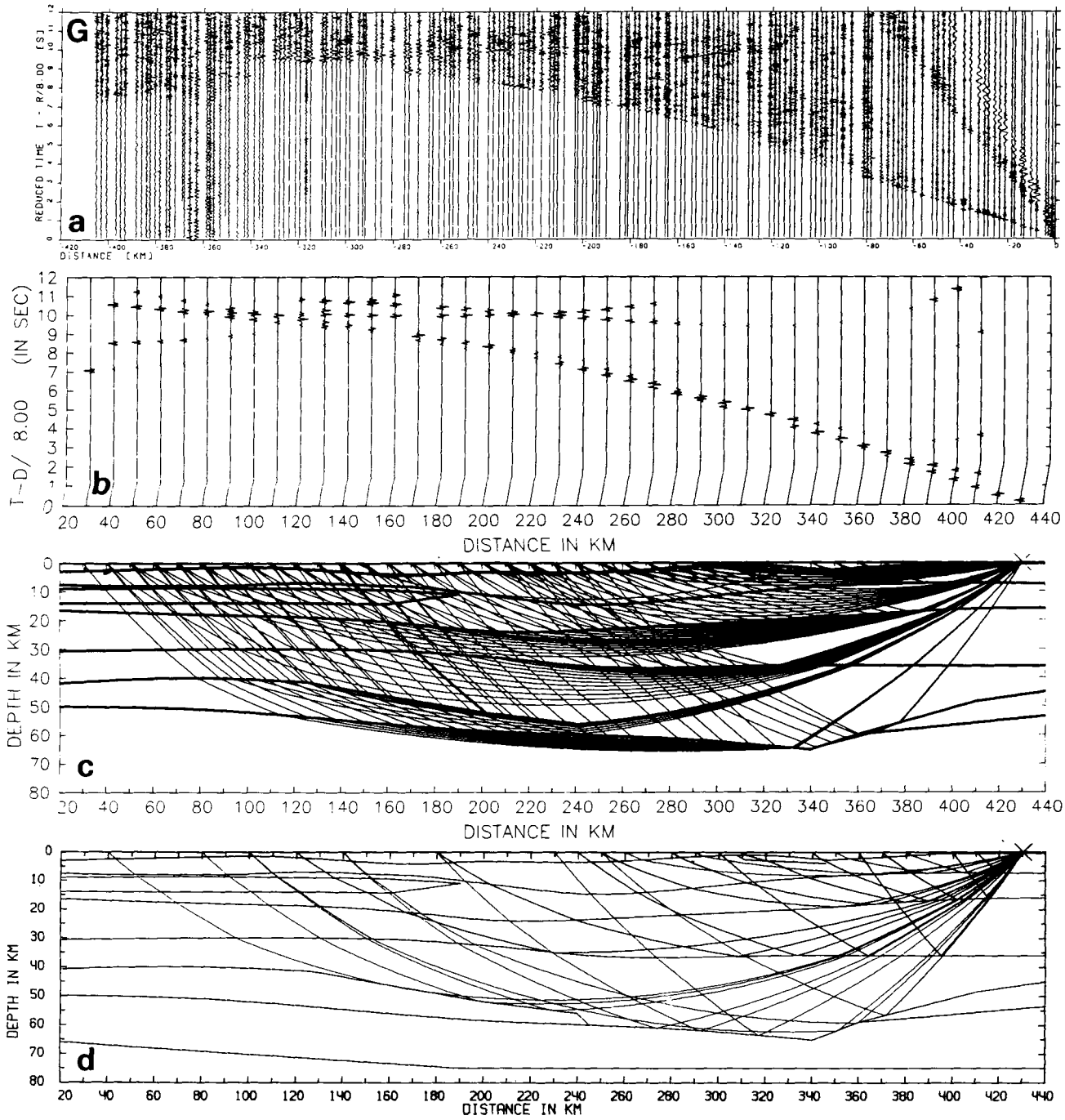

Figure 8. See caption to Fig. 2.

southern part. Local low- and high-velocity zones and variations of V_P/V_S occur along the profile with distance and depth. It should be noted, that by merely analysing the traveltime curves of the first arrivals, only a fraction of the kinematic information is used and therefore, a cross-section without the first-order interfaces is produced. Therefore, the reflected waves reliably correlated in the observed wavefields have no analogous arrivals in the computed wavefields of these models.

The final stage of the interpretation was to apply the 2-D dynamic ray-tracing technique. The SEIS83-program package (Červený & Pšenčík 1983) and programs developed by Azbel, Dmitriyeva & Yanovskaya (1981) were used. An initial 2-D model was constructed using the information described above and also 1-D models calculated by the direct method of trial and error (see Luosto & Korhonen 1986). The ray diagrams, traveltime and amplitude curves and synthetic seismograms of refracted and reflected waves of the final model have been computed for each source (Figs 2–8, 11). The computed and observed traveltimes for the final model of the first arrivals coincide within the limits of 0.1–0.15 s.

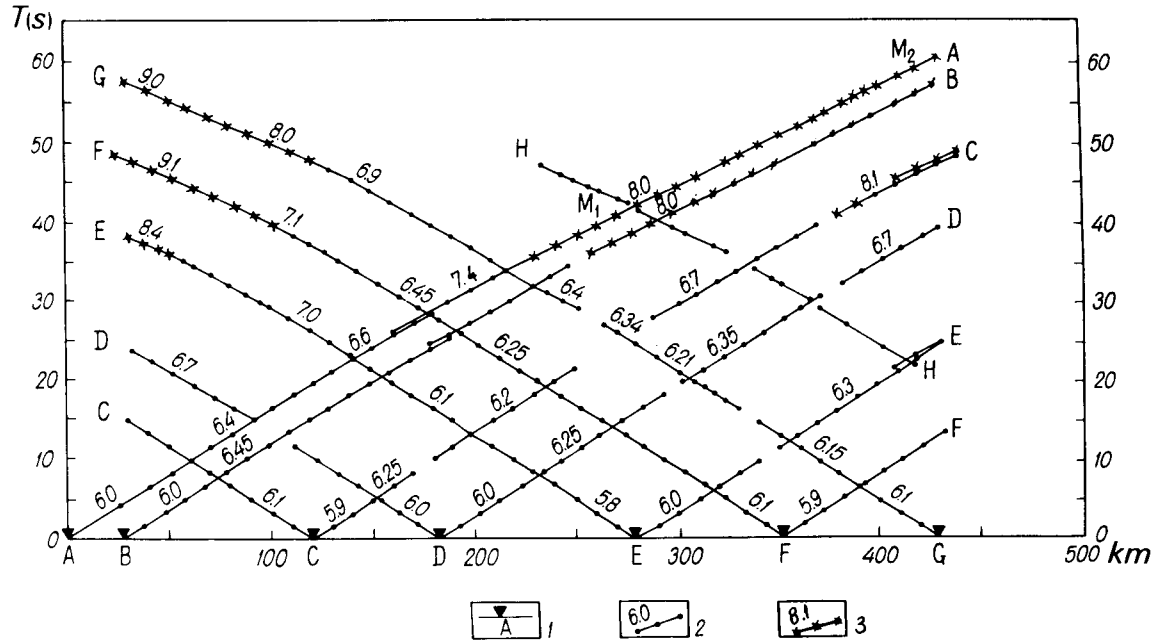

Figure 9. Traveltime curves obtained on the Baltic profile. 1—shotpoint (SP), 2—crustal wave with apparent velocity, 3—mantle wave.

MAIN RESULTS

The combined results achieved by different methods are presented in Fig. 16 and illustrate the main structural features of the crust and upper mantle along the profile. The first section (Fig. 16a), obtained by ray tracing, presents the *P*-wave velocity distibution and the reliefs of the interfaces. The second section (Fig. 16b) shows the locations of reflecting elements in the cross-section independently constructed from traveltimes of the most intensive *P* and *S* phases by prospecting methods. Also included are isolines of average velocities based on the 1-D solutions. The third section (Fig. 16c) gives the Bouguer gravity anomaly along the profile, the values of the ratio t_S/t_P for reflected P^MP and S^MS waves for individual shotpoints (see also Table 3) and the isolines of the ratio V_P/V_S for the first arrivals of

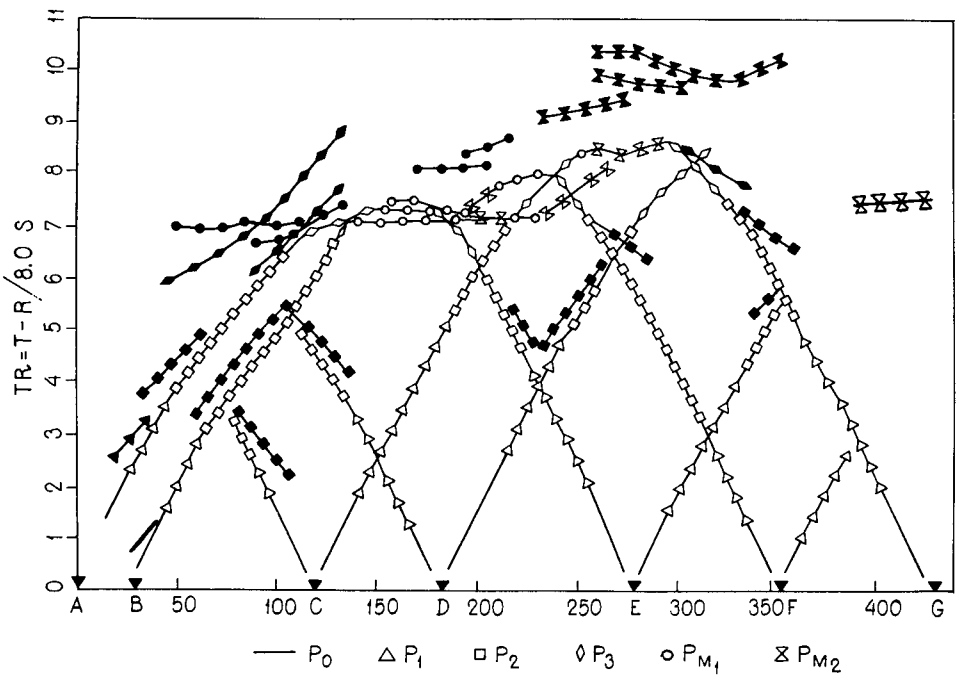

Figure 10. Reduced traveltime curves for refracted (open symbols) and reflected (filled symbols) waves versus half distances from shotpoints, $V_R = 8\ \mathrm{km\ s^{-1}}$.

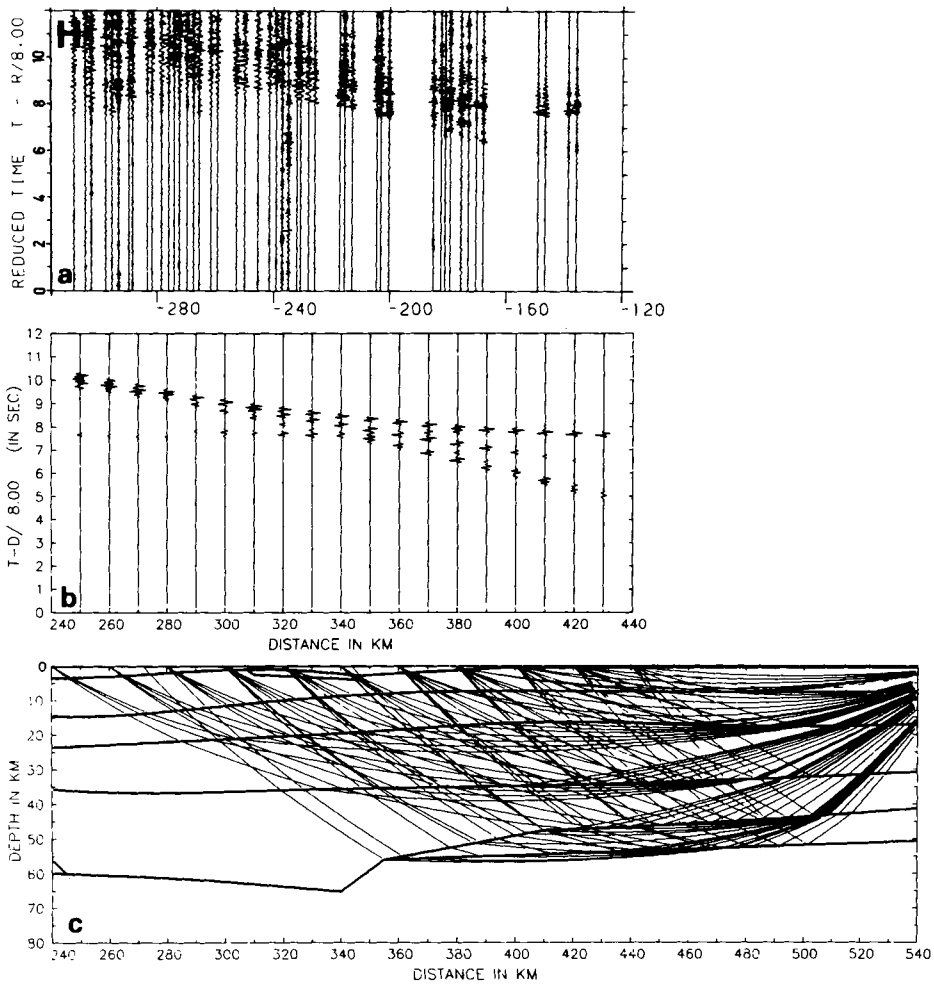

Figure 11. The 2-D modelling for shotpoint H along the Baltic profile, (a) amplitude normalized observed *P*-wave record section, bandwidth of digital filter 2–15 Hz; (b) amplitude normalized synthetic record section; (c) ray paths in the model. For more information see Figs 2–8.

Table 2. The characteristics of main groups of *P*- and *S*-waves.

SP Wave	A_N	B_N	C_N	C_S	D_N	D_S	E_N	E_S	F_N	F_S	G_S	H_S	Interval of registration (km)
					Velocities (km s^{-1})								
P_0	–	6.0	5.9	6.1	5.8–6.1	6.0	6.0	5.8	5.9	6.1	6.1	–	0–40–60
P_1	6.4	6.4	6.2	6.3	6.2	6.4	6.3	6.1	6.3	6.3	6.2	–	0–80–100
P_2	6.6	6.5	6.7	6.4	6.4	6.7	–	6.5	–	6.3	6.4	6.4–6.7	100–200
P_3	7.4	7.4	7.1	–	6.7	–	–	7.0	–	6.4	6.7–7.1	6.7	200–280
P_{M1}	8.0–8.1	8.0	8.1	–	–	–	–	8.4	––	7.1	8.0	8.0–8.5	200–380
P_{M2}	8.5	8.5	–	–	–	–	–	–	––	9.0	9.0	–	300–430
S_1	3.5	3.6	3.5	3.6	3.6	3.6	3.4	3.5	––	9.0	3.4–3.7	–	0–40
S_2	3.6	3.7	3.8	–	–	3.8	3.6	3.6	––	3.8	3.6–3.8	–	40–80
S_3	3.8	3.9	3.7	–	–	3.9	–	3.8	––	–	3.7–3.8	–	80–180
R_c^*	200	220	260	–	–	–	–	220	––	–	280	230	
t_{cr}^*	7.0	7.1	8.4	–	–	–	–	7.3	1.61	240	8.3	7.4	
t_S/t_P	1.72–1.75	1.64–1.72	1.72–1.75	–	1.70	–	1.69	–	1.70	8.0	1.67		0–100
	1.74–1.76	1.73	1.67–1.69		1.70	–	1.71	–	1.71		1.71		100–200

* R_c—cross-over distance of mantle waves, t_{cr}—time reduced with velocity of 8.0 km s^{-1} at point R_c.

Table 3. The ratio t_S/t_P for the main phase of reflections from the M boundary.*

SP	X km	t_s/t_p	SP	X km	t_s/t_p	SP	X km	t_s/t_p	SP	X km	t_s/t_p
A	47	1.85	B	78	1.79	D_S	103	1.76	C_N	200	1.76
	60	1.80		103	1.78		112	1.78		210	1.76
	75	1.81		115	1.76		120	1.78		220	1.76
D_N	255	1.73	F_S	289	1.75	G	280	1.75	H	479	1.71
	277	1.73		254	1.75		260	1.76		486	1.70
	360	1.73		226	1.78						

*) The X is the position of reflection point for laterally homogenous structures. It is equal to half the distance (R) between shotpoints and receivers plus the X-coordinate of the source or $X = X_{source} + R/2$.

refracted waves calculated by the method of generalized inversion.

The boundaries shown by thick lines in Fig. 16(a) should not necessarily be considered to extend from end to end in the profile, because we have observed reflections coinciding with calculated traveltimes and amplitudes only from those parts of the boundary marked with special signs. The crustal model is composed of five layers extending along the profile and separated by curved interfaces (Fig. 16a). The thickness of the first layer varies from 0.5 km (between shotpoints E–F) to 4 km in the zone between SP C–D. The velocity changes from 5.8 to 6.1 km s^{-1}. This layer allows us to compare the known velocities of the surface rocks with the velocities estimated on the basis of the first waves of the records near the source. Fig. 17 clearly shows the areas where the surface velocity is less than 6.0 km s^{-1} or higher (e.g. the vicinity of points $X = 280$ and $X = 320$ km, respectively). The existence of a high-velocity body (Fig. 16a) between shotpoints E and F ($V = 6.4$ km s^{-1} down to 3 km depth) is associated with the Outokumpu ore

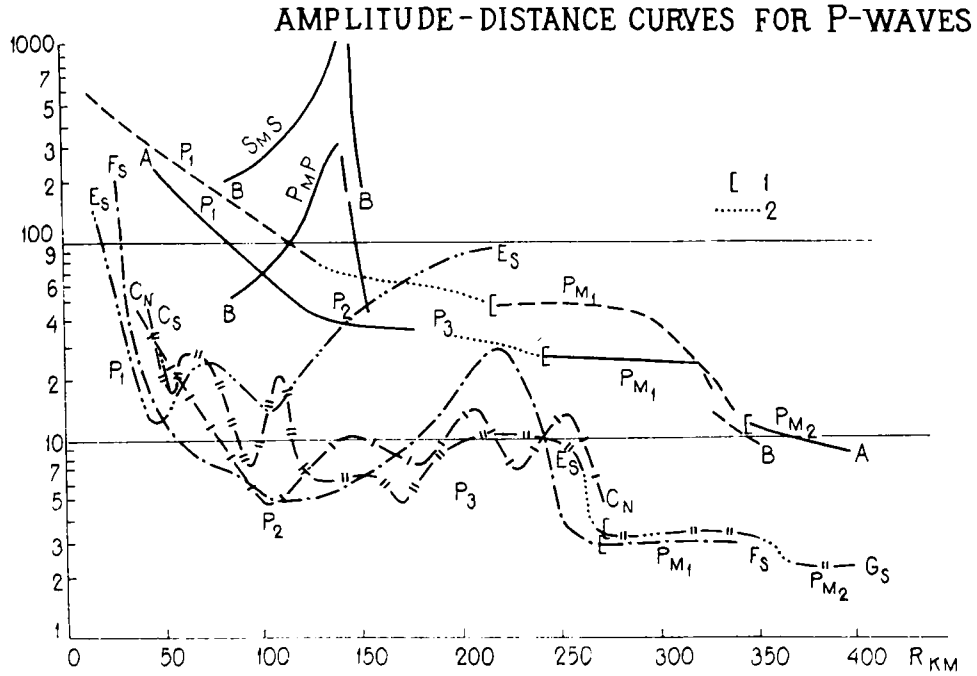

Figure 12. Observed amplitude curves for shotpoints A–G, subscript N or S refer to the direction north or south from the shotpoints; 1—cross-over distance for mantle waves; 2—interpolation between observations; P_1, P_2, P_3—crustal waves, P_{M1}, P_{M2}—mantle waves, P_MP, S_MS—Moho reflections of *P*- and *S*-waves.

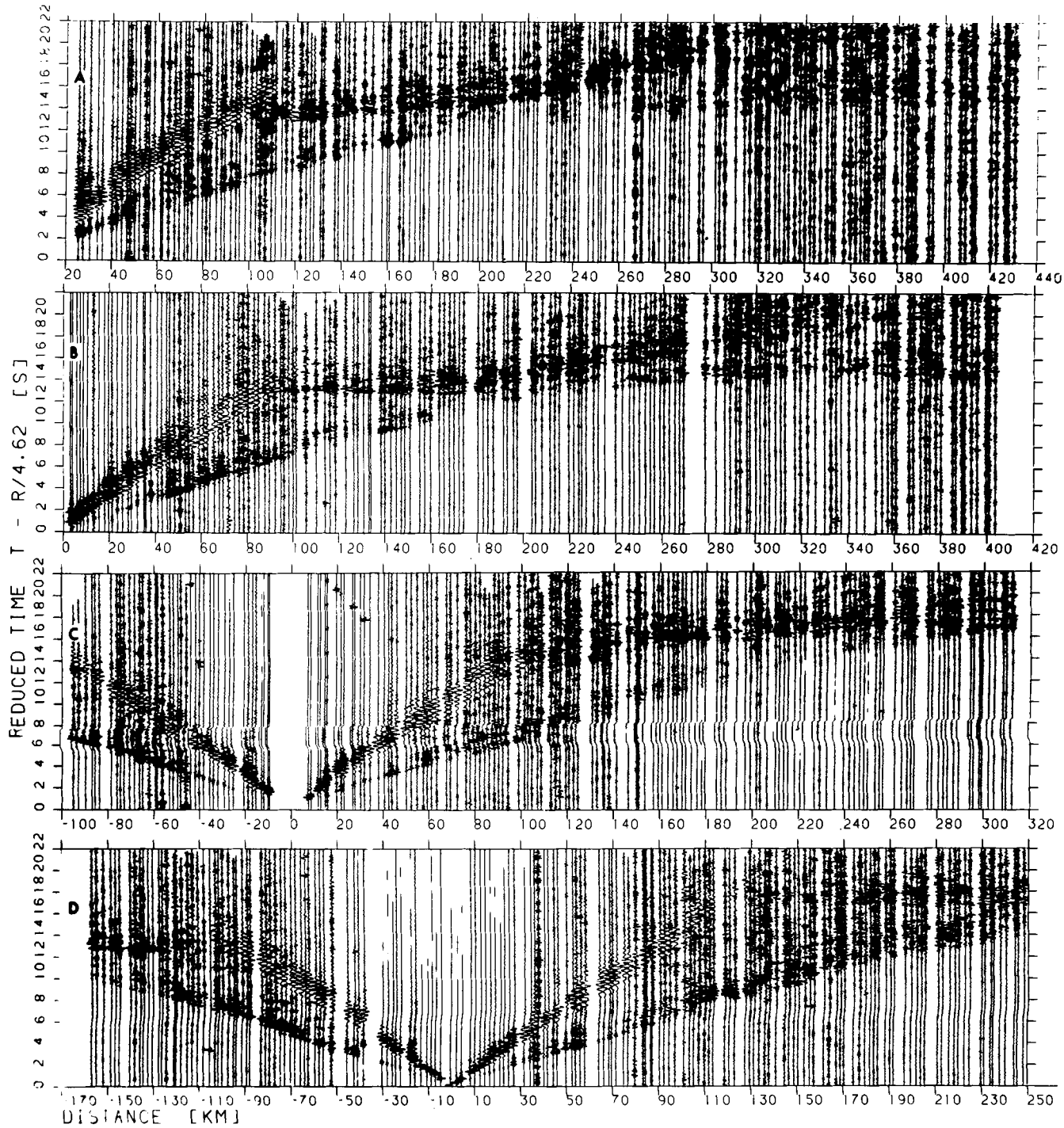

Figure 13. Amplitude normalized *S*-wave record sections for shotpoints A–G. Bandwidth of digital filter 2–6 Hz. Reduction velocity 4.62 km s^{-1}.

formation (Koistinen 1981). The direct indication of the deposit is the emergence of the first arrivals with an apparent velocity of 6.4 km s^{-1} between shotpoints E and F whereas most of the arrivals from the same depths have velocities of 6.1–6.2 km s^{-1}. Moreover there is a shadow zone in the wavefields of shotpoints D and G (Figs 5 and 8) caused by the change of propagation paths of the refracted waves enveloping this body. The distribution of average velocity (Fig. 16b) also indicates the presence of a body whose roots possibly go even deeper. But because the distance between shotpoints E and F is 70 km only a more detailed investigation will clarify this structure in more detail. The velocity contrast through the boundary K_1 does not exceed 0.3 km s^{-1} and varies slightly along the profile.

The depth to the bottom of the second layer (K_2) is almost the same (8 km) in the northern and southern parts

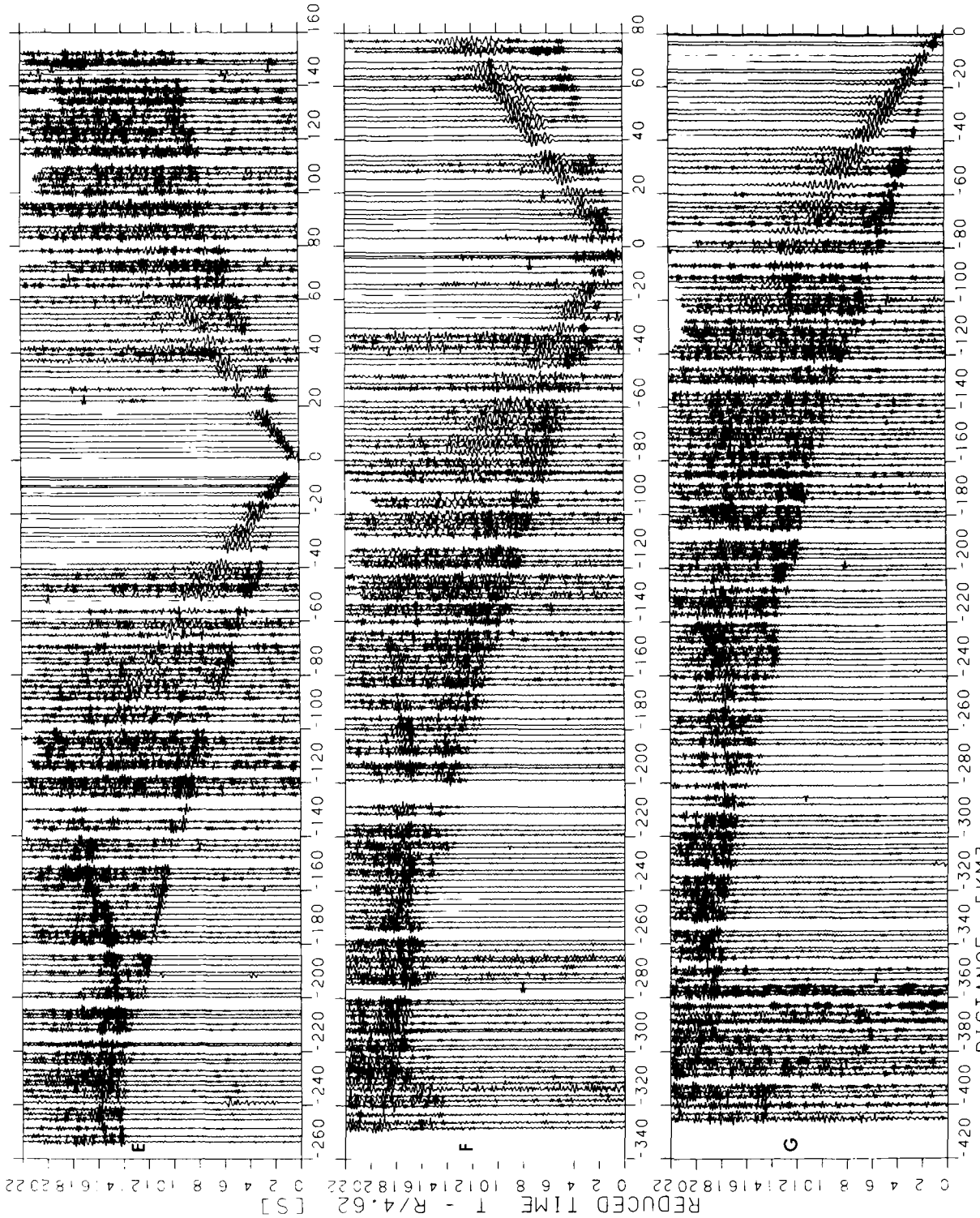

Figure 13. (*continued*)

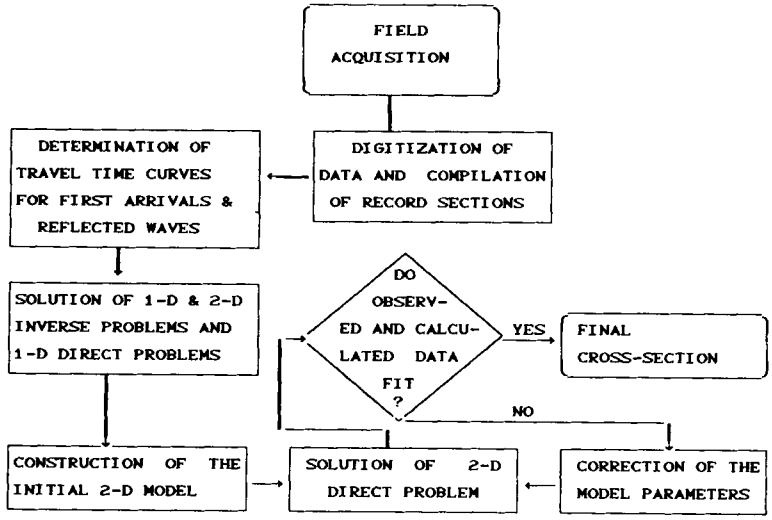

Figure 14. DSS data processing and interpretation steps.

of the profile. However it is greater in the central part, being 15 km. The vertical velocity gradient bears an inverse relation to the thickness, varying from 0.02 to 0.01 s^{-1}. The shapes of the velocity isolines (not shown in the figure), e.g. 6.2 km s^{-1}, are similar to the relief of the lower boundary of the layer (see Fig. 16a).

The third layer, with velocities from 6.3 to 6.45 km s^{-1}, has a thickness of about 10 km. The lateral velocity variations are most marked in this layer. Actually it includes a high-velocity layer ($V = 6.5$ km s^{-1}), in the southern part wedging in the vicinity of shotpoint D. This layer enables us to explain simply the main features in the reversed wavefields from shotpoints A, B, C_S and D_S. At the distance of about 80 km from shotpoints A and B, the apparent velocity of the first arrivals suddenly increases which at longer distances is the cause of systematic decrease of traveltimes compared to the traveltimes from the other sources. A sharp attenuation of these waves is seen at distances exceeding 140 km from the shotpoints A and B (see Fig. 2). The upper boundary strongly reflects waves from shotpoints A, B, C_S and D_S being clearly seen in the records (Figs 2–5) whereas they are not observed for shotpoint D_N. The wedging is indirectly indicated also by a sudden change in character of the field for supercritical reflections from the M boundary, recorded at 300–320 km for shotpoint A and 260–280 km for shotpoint B. This is more clear in the *S*-wave record sections (Fig. 13). The zone of wedging is well outlined as a velocity gradient variation area (Figs 3 and 4) and is revealed in a considerably greater value of $t_0(R/2)$ for the isoline $V = 6.5$ km s^{-1} (Fig. 15a).

The middle crust consists of a thick layer of 15–20 km in which the velocity varies from 6.6 to 6.8 km s^{-1}. In the south, the velocity gradient is approximately three times bigger than in the northern and central parts. The layer is traced by refracted rays generated from SP A, B, F, G and emerging as the first arrivals at distances of 140–200 km from the source. In the case of shotpoints C, D and E, these waves behave almost like the head waves i.e. they do not penetrate deeper than 3–5 km under the upper boundary of the layer (see ray diagrams in Figs 4 and 5).

The distinct boundary in the top of the lowest layer in the crust at a depth of 30 km has been identified from reflected *P*-waves registered in the record sections from shotpoints A, B, C and E. Thus, on the record section for shotpoint A at 100–160 km, there are weak later arrivals 1 s earlier than the marked reflections from the M boundary. The intensity of these arrivals with an apparent velocity of 6.5 km s^{-1} increases at 180–240 km and the time difference relative to the first arrival is more than 1 s. Similar arrivals recorded from shotpoint B are easily visible behind the first arrivals with the same time delay at the 220–260 km interval (Fig. 3). In the record sections for shotpoints C_N and D_N, an intensive one-cycle oscillation with a 0.5 s delay relative to the first arrivals and a velocity of 6.7 km s^{-1} (Figs 4 and 5) was recorded at 160–240 km from source. These arrivals can be interpreted as the same as the branches from shotpoints A, B and E in the reverse direction but their amplitudes are significantly smaller (Fig. 6). The depth of the boundary in the model varies from 30 to 36 km, the velocity contrast is 0.25 km s^{-1} in the south and 0.15 km s^{-1} in the northern part of the profile.

The thickness of the lowest crustal layer varies considerably along the profile: in the central part it reaches 30 km, decreasing to 10 and 12 km in the southern and northern parts, respectively. The velocity of *P*-waves increases with depth from 7.0 to 7.3–7.5 km s^{-1}. In the central part the vertical component of the velocity gradient has its smallest value 0.008 s^{-1}, while in the south it increases to 0.018 s^{-1}. The velocity in the lowest part is the most uncertain because the refracted rays do not penetrate the whole layer (compare Figs 2, 3, 7, 8 and 4, 5). The branches of traveltime curves observed with velocities of 7.2–7.3 km s^{-1} have been obtained only for shotpoints A, B and G.

The main features of the first mantle waves with V greater than 8.0 km s^{-1} (see Fig. 10), with distinct differences in the slope of reversed traveltime curves at distances over 200 km are reasonably explained by the velocity structure of the upper mantle and the relief of crust–mantle boundaries shown in Fig. 16(a). There are two boundaries in the transition zone from crust to mantle in the model: the upper M_1 or Moho with a velocity of 8.0 km s^{-1} and the lower M_2

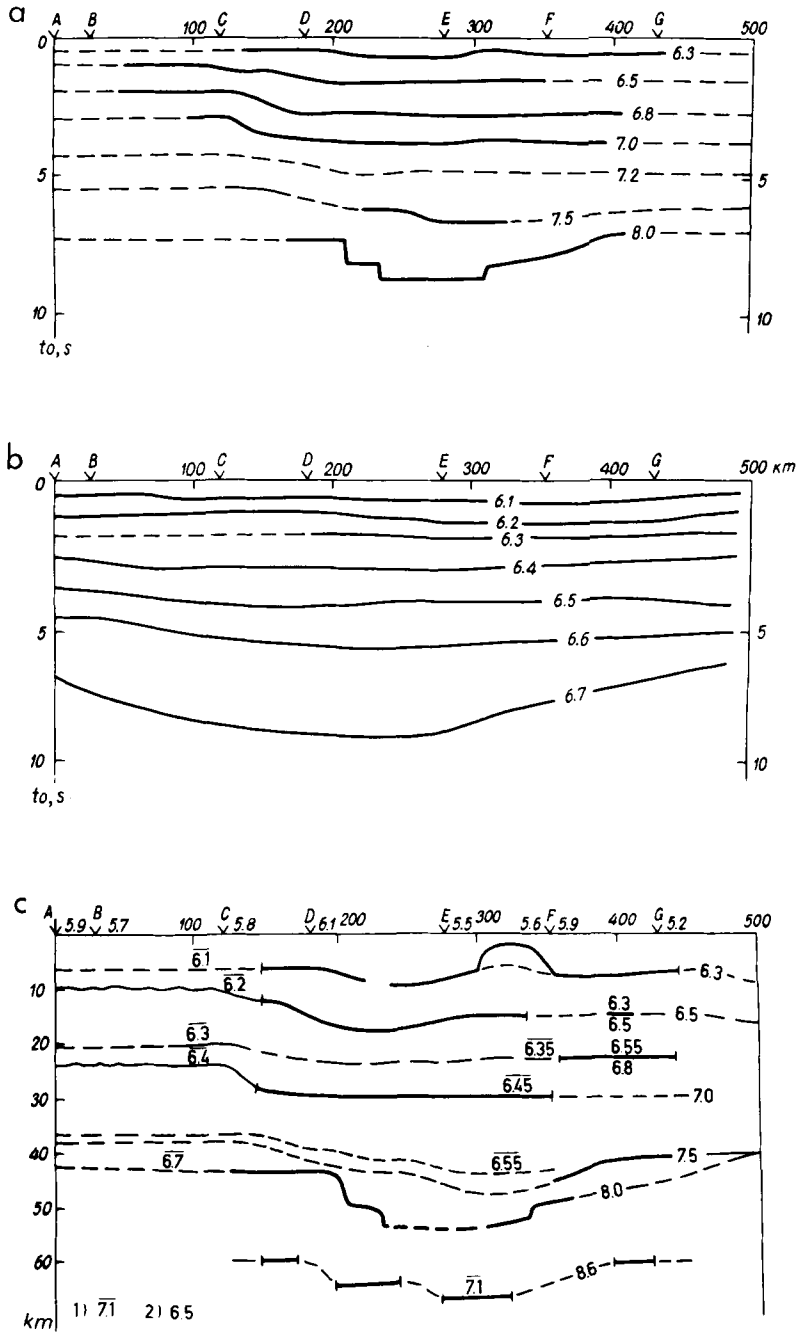

Figure 15. Initial 2-D model by the intercept-time method. (a)—velocity isolines as a function of distance and intercept time, (b)—isolines of average velocities between the Earth's surface and the isoline determined by 1-D solution for every shotpoint, (c)—velocity cross-section; 1 = average velocity, 2 = velocity *in situ*.

with a velocity of 8.4–8.5 km s^{-1}. As a whole the structure of transition from crust to mantle has a grabenlike shape with a significant depression in central part, where the transitional layers below the Moho from south and north are wedged and therefore M_1 and M_2 coincide. According to the model, the depth of Moho there varies from 60 km ($X = 270$ km) to 65 km ($X = 340$ km); the velocity contrast is $8.5–7.3 = 1.2$ km s^{-1}. The refracted mantle waves from shotpoints A, B, C and F, G originate from this part of the boundary. Their depth of penetration in the mantle is not more than 70 km. The calculated waves reflected from the deepest part of the Moho have maximal amplitudes for the later arrivals (Figs 2–4, 7 and 8) which is in good agreement with observations. The calculated and observed traces with maximal amplitudes practically coincide at the following intervals: 380–420 km for shotpoint C, 400–430 km for D, 180–240 km for F and 140–280 km for G.

To the south and north the M_1 boundary rises sharply and the transition layers below are revealed with velocities of 8.0–8.2 km s^{-1} (gradient 0.029 s^{-1}). In the southern part up

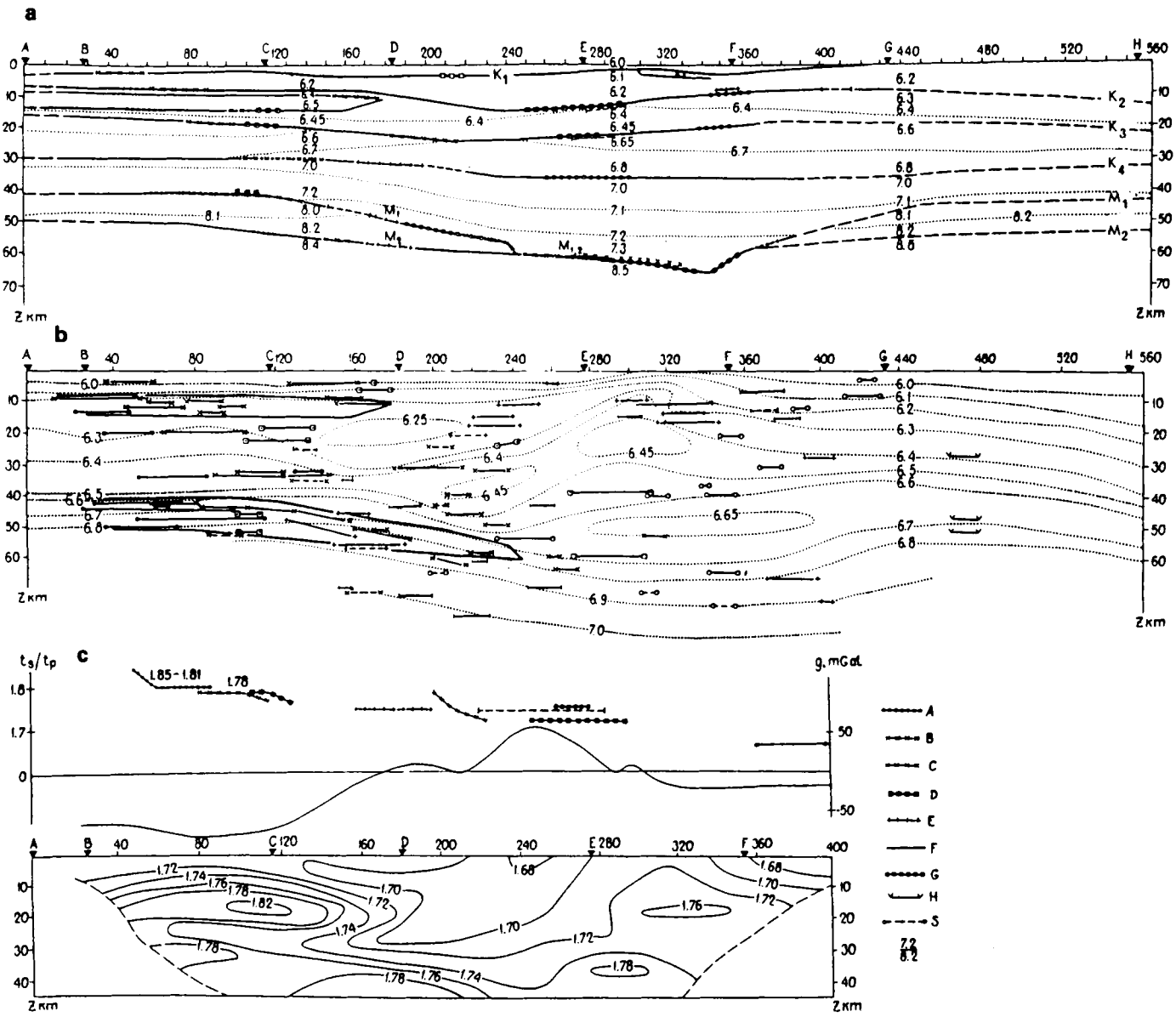

Figure 16. Summary of results along the Baltic profile. (a) Final model obtained by ray tracing. Thick lines $K_1, \ldots, K_4$—velocity boundaries in the crust; M_1—Moho; M_2—another discontinuity in the upper mantle; marked parts of boundaries correspond to observed reflections on the records; dotted line—velocity isoline, (b) *P* and *S* reflectors and isolines of average velocity of *P*-waves, (c) Bouguer gravity anomaly along the profile, t_S/t_P values of Moho reflections and isolines of ratio V_P/V_S, along the profile.

to $X = 130$ km the depth of the upper boundary M_1 is about 40.5 km and it is practically horizontal, then it goes linearly down to $Z = 58$ km at $X = 270$ km. The *P*- and *S*-waves reflected from the M_1 boundary dominate and correspond to the observed fragments of traveltime curves for shotpoints A and B at distances of 100–200 km from the source. The calculated reversed branches for shotpoints C and D agree with the values for the intensive later arrivals correlated with the short interval $X = 30$–60 km of the profile. The waves reflected from the M_2 boundary have a 0.5 s delay to reflections from the M_1 boundary at interval 180–220 km and coincide with them at greater distances.

A proposed similar transitional layer in the northern part of profile is not so firmly based on observations. The distance between shotpoints F–G is only about 80 km and over a distance of approximately 125 km between shotpoints G and H there were no recording stations. Only the analysis of traveltimes of the first and later arrivals for shotpoint H (see Fig. 11) and a comparison with calculated values enabled us to draw roughly a transition layer with a strongly reflecting boundary at a depth 45 km with a sharp slope to the central trough (Fig. 16a).

We would like to point out one more peculiarity in the observed wavefield, which is probably connected with the crust–mantle transition zone: the duration of wave packages of reflected waves exceeds 1.5–2 s in records of shotpoints A, B and C. Their amplitudes are rather high and stable. These features are impossible to explain within the framework of a model with one first-order boundary between the crust and the mantle. More probably, there is a

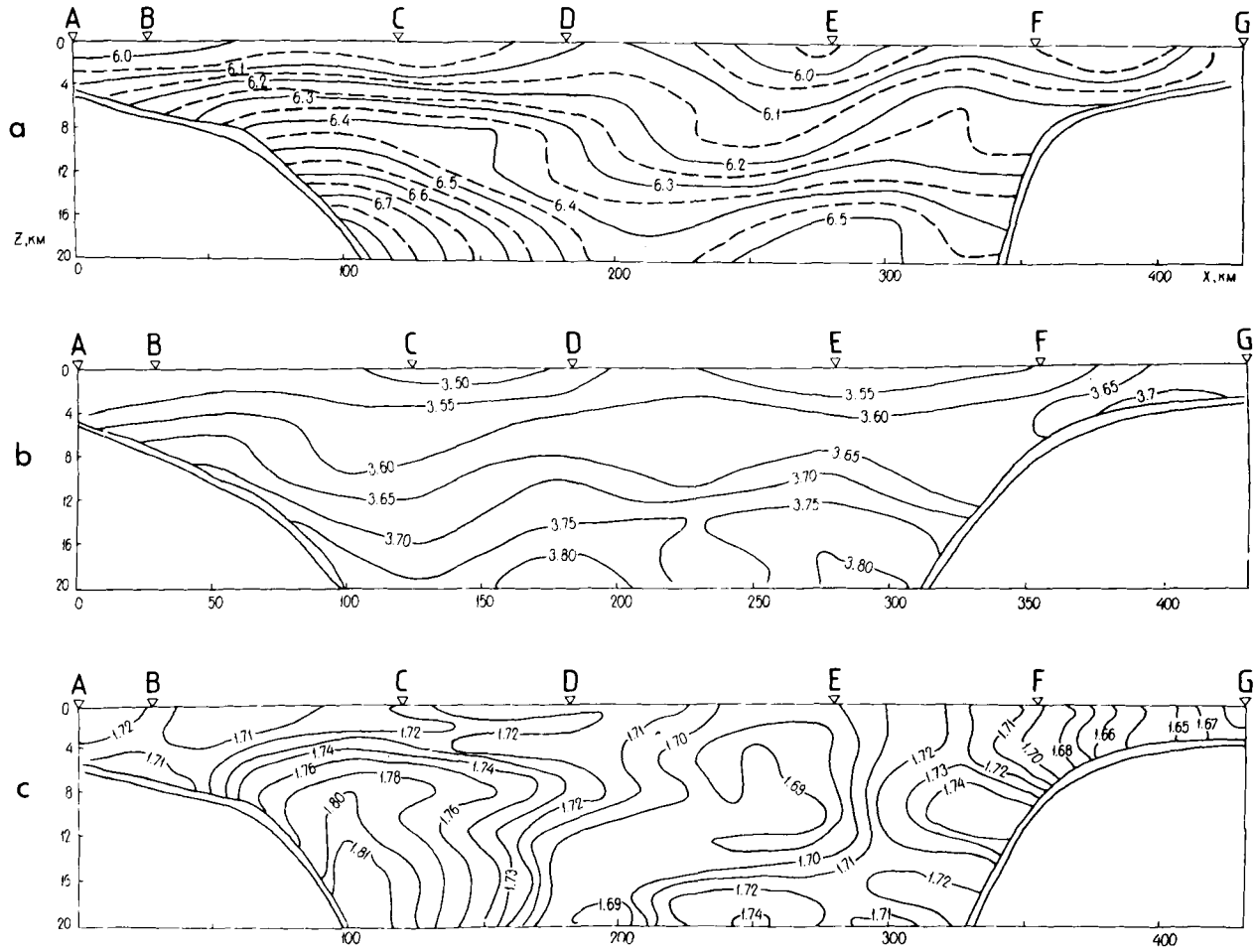

Figure 17. The velocity structure of the upper part of the crust computed by a generalized inverse method. (a)—isolines of V_P; (b)—isolines V_S; (c)—isolines V_P/V_S.

zone below the Moho consisting of thin layers with high and low velocities and the observed multiphase oscillation is a result of the interference of transmitted and reflected waves on the inner interfaces with the stack.

DISCUSSION

The seismic data presented above show differences in the structure of the crust and upper mantle between the southern, central and northern parts of the profile, thereby supporting the separating of the lithosphere into three blocks as introduced in an earlier paper (Luosto *et al.* 1985). The block structure of the crust is revealed in the relief of the M_1 boundary, the character of velocity increase with depth, as well as in the degree of stratification of the crust. The Moho is deepest in the central block and decreases dramatically in the transition zones between this block and the adjacent ones to the north and south. The crust–mantle boundary is quite sharp so that the velocity contrast in the central block at a depth of about 60–65 km approaches 1.2 km s^{-1}. The lower crustal layer in the central block is characterized by a comparatively large thickness and high velocity of *P*-waves (over 7.0 km s^{-1}) in the lowest crust. The velocity gradient in this block is smaller compared to the other blocks. (Figs 17a and 16a).

The structure of the crust and mantle for the southern block is very individual and more stratificated than the others (Fig. 16b). In the upper crust at a depth of 8–14 km a high-velocity layer is revealed ($V = 6.5$ km s^{-1}) which seems to be thrust in a thicker layer with a velocity of 6.3–6.4 km s^{-1}. The many reflecting elements calculated from the separate traveltime fragments of later arrivals emphasize a layered structure with distinct boundaries. The lower crustal layer here is considerably thinner and has a higher velocity gradient than in the central block. The depth of the M_1 is about 40 km and the velocity contrast is 0.8–1.0 km s^{-1}. M_2, the deepest reflecting boundary already in the upper mantle at 50 km, is practically horizontal up to $X = 130$ km after which it dips sharply in the transition zone between the southern and central blocks (see Fig. 16a). The influence of this structure is clearly seen in the records of the first arrivals of mantle waves (shotpoints A, B, F, G) as well as in the shape of the traveltime curves and the time of intersection of the crustal and mantle branches for the first refracted waves (see Table 2).

The southern block shows the highest value for the V_P/V_S ratio, 1.8 up to M_1. In the central block the ratio is near to normal at 1.73, and in the northern one the value is lowest being 1.68. The anomalously high ratio for V_P/V_S of 1.78–1.80 within the 15–40 km depth interval in the south

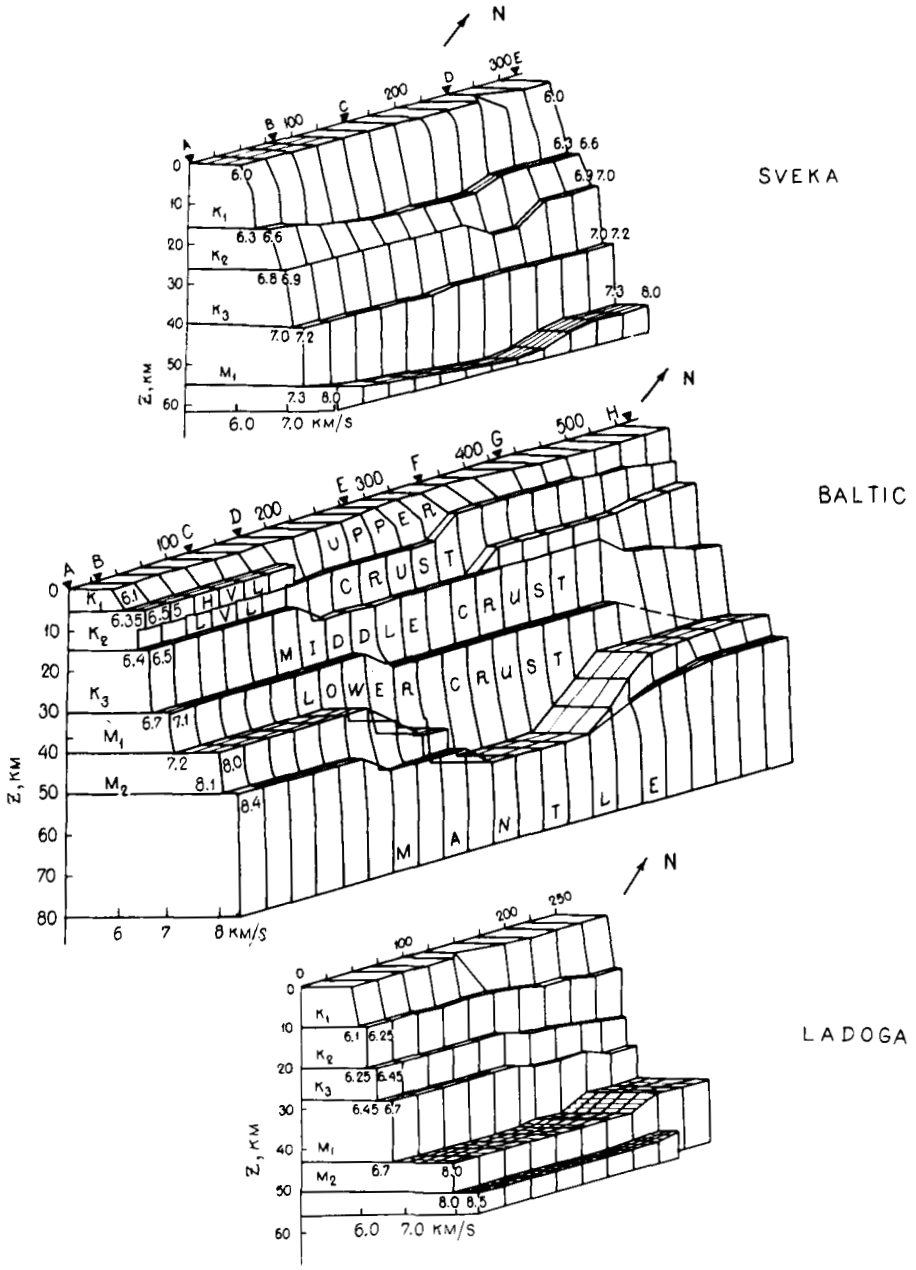

Figure 18. Simplified velocity diagrams for DSS profiles in the SE Fennoscandian Shield. Results from Grad & Luosto (1987) and Litvinenko *et al.* (1987) are adapted for diagrams of the Sveka and Ladoga profiles.

could be due to the higher plasticity of the intrusive body, which has been preserved since the time of its formation.

Because the observation system does not provide sufficient overlapping of the traveltime curves, it was impossible to trace the exact positions of the boundaries between the blocks. Nevertheless, the observed wavefield features combined with the characteristics seen in the cross-section enable us to make some remarks about the tectonic nature of the contact zones between blocks which are probably zones of mantle origin. A comparison of the results with the geotectonic provinces on the geological map (Fig. 1) shows that the northern, central and southern blocks correspond to the Karelian province of Archean age, the Ladoga–Bothnian Bay zone and the expanded area of Rapakivi granites in the younger Svecofennian province, respectively.

The structure of the Ladoga–Bothnian Bay zone is the best studied because the three DSS profiles cross this area: Sveka, Baltic and Ladoga (Fig. 1). The depth of the M boundary in this zone was first estimated from observations made on 'Sveka' (Luosto *et al.* 1984). But this profile was not long enough to determine details of the transition zone to the Karelian block in the northeast or to a granitic massif in the southwest. The velocity cross-section of 'Sveka' (Grad & Luosto 1987) and 'Baltic' (Fig. 18) have similar features as far as the relief of M boundary and high velocities in the lowest part of the crust are concerned. The depth of the boundaries (M_1 and M_2) on the Ladoga profile are 40 km

($V = 8.0\,km\,s^{-1}$) and 50 km ($V = 8.5\,km\,s^{-1}$) respectively (Litvinenko *et al.* 1987) and are more similar to the characteristics of the northern than to the central block of 'Baltic'. All the boundaries are practically horizontal on the Ladoga profile. In the Moho there is a small upward step when crossing to the Karelian block. If we compare the record sections from *SP* H on the Baltic profile with the Bothnian profiles in middle part of Finland, Fig. 1., (Yliniemi 1989; Yliniemi & Luosto 1988), it can be assumed that the Moho boundary on the northeastern continuation of the 'Sveka' has the same sharp uplift as it has in the 'Baltic'. Thus in the southeast the Ladoga–Bothnian trough is limited by a rise of the mantle block, the amplitude of which is approximately 20 km, whereas the horizontal length of the transition is not more than 30–50 km. In the northeast direction a rise of similar amplitude seems to slope more gently. Another interesting feature can be seen when comparing the Sveka, Baltic, Kem–Tulos and Ladoga profiles. The velocity cross-sections are almost the same in the upper crustal part in the Karelian province, but there are obvious differences in the lower crust: in the Karelian profiles the thickness of the lowest layer of the crust does not exceed 15 km and the maximal velocity of the *P*-wave is $6.8\,km\,s^{-1}$, while in the Finnish profiles such a velocity corresponds only to the upper boundary of this layer increasing up to $7.3\,km\,s^{-1}$ or possibly even more to the M discontinuity. The southwestern boundary of the Ladoga–Bothnian Bay zone in the Svecofennian province resembles the northeastern one with respect to the M relief and the thickness of the lower crust. The following specific features in the structure of the southern part of the 'Baltic' may be connected with the origin and development of the Rapakivi massif; the high-velocity layer at the depth 8–10 km, the *low S-wave velocities*, the sharp decrease of velocity gradient in the upper crustal part up to 20 km, the smaller thickness of whole crust and the existence of intermediate crust–mantle layer at a depth of 30–40 km.

Finally it is interesting to compare the seismic results with the Bouguer gravity anomaly along the profile (Fig. 16c). It is obvious that the curve does not correlate completely with the relief of seismic boundaries: the negative anomaly in the southern part of 'Baltic' coincides with the smallest crustal thickness relatively to the central part, where the gravity anomaly is positive. But if we assume that the ratio V_P/V_S reflects the state of rocks, high values correspond to low density and greater plasticity, then the coincidence of the high ratio 1.8 for V_P/V_S and the negative Bouguer anomaly in the southern and opposite situation in the central block offers a physical interpretation.

CONCLUSIONS

(1) The crustal structure observed along the Baltic profile reveals considerable changes in crustal thickness and in the physical properties of the crust. The crust is unexpectedly thick, more than 60 km in the middle of the profile, where it crosses the Ladoga–Bothnian Bay zone situated in the border region of Archean and Proterozoic domains. In the south below the large Viborg Rapakivi intrusion the crust is only about 40 km thick. Also in the NE part of the profile the crust is thinner, with a thickness of about 45 km.

(2) Velocity distributions on the profile indicate clear layered structure. In the upper crust the *P*-wave velocity varies from 6.0 to $6.4\,km\,s^{-1}$, in the middle crust from 6.5 to $6.8\,km\,s^{-1}$ and in the lower crust from 7.0 to $7.3\,km\,s^{-1}$. In the upper mantle the velocity is from 8.0 to $8.5\,km\,s^{-1}$; highest values are observed below the thickest part of the crust.

(3) Taking into account the variations of the crustal thickness and the velocity distribution the profile can be separated into three blocks, which coincide from the southwest to the northeast with geotectonic provinces of the Rapakivi intrusion, Ladoga Bothnian Bay zone and the Karelian province. The highest average *P*-wave velocities are observed in the southern block. In the central block *P*-wave velocities are smaller with the exception of the region of the Outokumpu copper deposit, where velocities for the uppermost crust are higher. In the south the *S*-wave velocities are extremely low with the average ratio of V_P/V_S being 1.8 and in the central block the ratio is near to normal at 1.73. In the northern block in the Archean granitoid gneiss basement, the *S*-wave velocities are high compared with *P*-wave velocities, resulting in a value of 1.68 for the V_P/V_S ratio.

(4) Comparing crustal thicknesses with those observed on adjacent profiles we can conclude that the Ladoga–Bothnian Bay zone together with its surroundings forms an anomalous region with an extraordinary thick crust in the low-altitude area.

ACKNOWLEDGMENTS

The authors are sincerely thankful for the excellent data to all the observers and the technical experts who participated in the field work or the data processing. We also thank Katriina Arhe for assisting with figure preparation and Annikki Lipponen for helping to improve an earlier version of the manuscript.

REFERENCES

Azbel, I. Y., Dmitriyeva, L. A. & Yanovskaya, T. B., 1980. *Algorithms and Programmes for Solutions of Direct Kinematic and Dynamic Problems for Waves Propagated in 3D Media* (in Russian), Academy of the Sciences of the USSR, Kola Branch, Geological Institute, Apatity.

Berckhemer, H., 1970. MARS 66-eine Magnetobandapparatur für seismische Tiefensondierung, *Z. Geophys.*, **36**, 501–518.

Burkhardt, H. & Vees, R., Explosions in shallow water for deep seismic sounding experiments, *J. Geophys.*, **41**, 463–474.

Burmin, V. Y., 1981. Numerical solution of the inverse one-dimensional kinematic seismology problem using the hodograph of refracted waves, *Izvestiya, Phys. solid Earth*, **17**, 922–926.

Buyanov, A. F., 1986. Generalized inverse technique in two-dimensional inverse kinematic seismic problem (in Russian), in *Mathematical Modelling of Systems and Phenomenon*, pp. 93–100 Academy of the Sciences of the USSR, Kola Branch, Geological Institute, Apatity.

Červený, V. & Pšenčík, I., 1983. SEIS83—numerical modelling of seismic wave fields in two dimensional laterally varying layered structures by the ray method, in *Documentation of Earthquake Algorithms by E. R. Engdahl*, pp. 36–40, World Data Center (A) for Solid Earth Physics, Report SE–35.

Grad, M. & Luosto, U., 1987. Seismic models of the crust of the

Baltic shield along the Sveka profile in Finland, *Ann. Geophys.*, **5B,** 639–649.

Koistinen, T., 1981. Structural evolution of an early Proterozoic strata-bound Cu-Co-Zn deposit, Outokumpu, Finland, *Trans. R. Soc. Edinburgh*, **72,** 115–158.

Korhonen, H., Luosto, U., Kosminskaya, I. P., Zverev, S. M., Sharov, N. V., Lund, C.-E., Ilmola, V.-M., Lanne, E., Tuppurainen, A. & Foursov, A. N., 1986. The international DSS profiles 'Fennolora' and 'Baltic' in Scandinavia (in Russian), in *Izucenie Glubinnogo Stroenija Vostocnoj Casti Baltijskogo Scita i Prilegajuscih Akvatorij Sejsmiceskim Metodami* (*Study of the deep structure beneath the eastern part of the Baltic shield and adjacent water areas by seismic methods*), pp. 38–55, Akademija nauk SSSR, Kol'skij filial, Geologiceskij institut.

Litvinenko, I. V., 1984. Seismic study of the Earth's crust of the Baltic shield (in Russian), Proceedings of the 27th International Geological Congress, Moscow 4–14, August, 1984, *Geophysics*, **8,** 9–20.

Litvinenko, I. V., Ankudinov, S. A., Gavrilov, I. A., Dvoretskyaya, L. M., Kalnin, K. A., Matveeva, N. N., Platonenkova, L. N. & Romanenko, N. G., 1981. Deep sections in the earth's crust of central Karelia and their seismic models (in Russian), *Zap. Leningr. gorn. Inst.*, **89,** 12–17.

Litvinenko, I. V. *et al.*, 1987. Deep seismic sounding in the Kola peninsula and Karelia (in Russian), in *Litosfera Central'noj i Vostocnoj Evropy, Geotraversy I, II, V,* pp. 21–32 ed. Cekunov, A. V., Akademija nauk ukranskoj SSR, Institut geofiziki, Naukova Dumka, Kiev.

Luosto, U., 1986. Reinterpretation of Sylen-Porvoo refraction data, *Report S-13,* Institute of Seismology, University of Helsinki.

Luosto, U. & Korhonen, H., 1986. Crustal structure of the Baltic shield based on off-Fennolora refraction data, *Tectonophysics*, **128,** 183–208.

Luosto, U., Lanne, E., Korhonen, H., Guterch, A., Grad, M., Materzok, M. & Perchuc, E., 1984. Deep structure of the Earth's crust on the Sveka profile in central Finland, *Ann. Geophys.*, **2,** 559–570.

Luosto, U., Korhonen, H., Kosminskaya, I. P., Zverev, S. M., Lund, C.-E., Sharov, N. V., Lanne, E., Tuppurainen, A., Ilmola, V.-M. & Foursov, A. N., 1985. First results from the DSS study on the Baltic profile in SE Finland, *Report S-11,* Institute of Seismology, University of Helsinki.

Nurminen, S. & Hannula, A., 1981. Deep seismic sounding equipment model PCM 1218-80, service guidance (in Finnish), *Report T-7,* Institute of Seismology, University of Helsinki.

Pavlenkova, N., 1973. Interpretation of refracted waves by the reduced travel time curve method, *Izvestiya, Phys. solid Earth,* **8,** 544–550.

Pavlenkova, N. I., 1982. The intercept-time method—possibilities and limitations, *J. Geophys.*, **51,** 85–95.

Puzyrev, N. N., 1959. *The Interpretation of the Seismic Data by the Method of Reflected Wave,* Gostoptekhizdat, Moskva.

Riznichenko, Y. V., 1985. *Seismic Prospecting of the Layered Media,* Nedra, Moscow.

Yliniemi, J., 1989. Seismic model of the Earth's crust along the Kemi-Kajaani line (in Finnish with English summary), in *XIV Geofysiikan päivät Helsingissä 3.-4. 5. 1989,* pp. 11–18, ed. Forsius, J., Geophysical Society of Finland, Helsinki.

Yliniemi, J. & Luosto, U., 1988. Seismic investigations of the earth's crust in the middle part of Finland (Abstract), in *Recent Seismological Investigations in Europe,* Proceedings of the 19th General Assembly of the European Seismological Commission, Moscow, October 1–6, 1984, p. 512.

Zverev, S. M., Boldyrev, S. A., Bourmin, V. Y. & Mironova, V. I., 1978. Weak earthquakes in the northern part of the Rift Zone of Iceland, *J. Geophys.*, **44,** 283–296.